Integrated Project - EUWB

Contract No 215669

Deliverable

D2.4.5

Multi-Source/Node Distributed Network Coded Modulation – Concepts, Structures, Algorithms and Performance Evaluation

Contractual data:	**M40**
Actual data:	**M41**
Authors:	**Jan Sýkora, Martin Mašek, Tomáš Hynek**
Participants:	**CTU**
Work package:	**WP2**
Security:	**PU**
Nature:	**Report**
Version:	**1.0**
Total number of pages:	**50**

Abstract

As the coexistence of different networks is an important issue, interference mitigation techniques were developed. However, contrary to the interference mitigation, interference can also be used in order to aid the communication of multiple devices in the same time and the same frequency band. This approach stems from the network information theory and wireless network coding. This deliverable deals with an application of Hierarchical Decode and Forward (HDF) strategy (originally developed for narrow-band systems) into UWB. An effect of several UWB-specific issues is investigated and described. A comparison to non–HDF approaches is also included.

Keywords

Wireless network coding, cooperative communication, ultra-wideband

Contents

List of Figures

List of Tables

Abbreviations

2WRC Two–way relay channel

AWGN Additive white Gaussian noise

BC Broadcast channel

BPSK Binary phase shift keying

C–SI Coplementary side–information

CIR Channel impulse response

DS Direct sequence

ED Energy detector

H–BC Hierarchical BC phase

H–MAC Hierarchical MAC phase

HDF Hierarchical decode and forward

HXA Hierarchical exclusive alphabet

HXC Hierarchical exclusive code

I.I.D. Independent and identically distributed

IMA Interference mitigation/avoidance

IR–UWB Impulse–radio ultra–wideband

ISI Inter–symbol interference

JDF Joint decode and forward

LDR Low data rate platform

MAC Multiple access channel

NC Network coding

PDF Probability density function

PPM Pulse position modulation

PSD Power spectral density

SNR Signal to noise ratio

TH Time–hopping

UWB Ultra–wideband

WNC Wireless network coding

XOR Exclusive OR operation

1 Executive Summary

Wireless network coding (WNC) is a promising approach to a multi–node/source communication. It allows nodes to exploit an interference of received signals to a rate increase which is, in fact, exactly opposite to an interference mitigation approach. WNC was originally developed for narrow–band (NB) systems. This deliverable deals with an application an necessary modification of WNC technique called Hierarchical Decode and Forward (HDF).

The goals of this deliverable are:

- Investigate the differences between NB and UWB systems in terms of HDF signal processing and considered UWB receivers.
- Introduce UWB–modified HDF signal processing considering the necessary modifications. We will consider both coherent and non–coherent receivers introducing different algorithms.
- Evaluate the performance in terms of capacity computation.

2 Introduction

2.1 Goals of the Report

This report provides results of an application of Hierarchical Decode and Forward (HDF) wireless network coding (WNC) strategy in impulse–radio ultra–wideband (IR–UWB) systems. This introduces a cooperation of communicating nodes on a physical layer. Here, we assume a two–way relay channel (2WRC) consisting of two end nodes and relay where WNC, namely HDF strategy, can achieve a double data rate compared to the conventional classical systems.

2.2 Problem Description

WNC is a technique enabling a cooperation among communicating nodes of a network yielding a better performance of the system. Idea behind is similar to a classical network coding operating on a network layer of the systems. Systems using NC can achieve better performance than the classical systems but this improvement is inherently limited compared to the possibilities of WNC. In NC, a cooperation takes place in such a way that the network topology is given and nodes are divided into end nodes (transmitting and receiving data messages) and intermediate relay nodes. A part of end nodes transmits messages intended to the other part of end nodes. These messages are received by the relay nodes, where the messages are combined, as well as by some end nodes from the other part. It is important that the messages at relay nodes are received separately before combining. Then the relay nodes transmit the combined messages to the part of end node awaiting the messages. The end nodes then decode the data intended to them from the combined messages and the knowledge of other end nodes' messages.

The difference between NC and WNC is that WNC operates on a physical layer and in such a way that the individual messages from end nodes are transmitted simultaneously and the combined data messages at relay nodes are received and decoded directly. However, this introduces many obstacles and difficulties due to the inherent variable nature of the wireless radio channel. This leads to a performance degradation under some conditions. Thus, the general goal of WNC is then to design such a signal processing at relay nodes that not only has a potential of performance boost but also which is inherently immune to the performance degradation by its nature.

2.3 Report Structure

The structure of the report is following:

- Section 3 gives a rough insight into the reason of application of HDF in UWB systems and describes the relation to EUWB project in terms of the comparison of possible approaches to cooperative cooperation.
- Section 4 introduces HDF strategy with its theoretical background and requirements necessary for its employment. It also includes a signal description used throughout the whole document.

- Section 5 describes some general UWB–related aspects assumed in this document, e.g. channel models, receiver types.
- Section 6 provides a more concrete description of assumed coherent HDF IR–UWB receiver, demodulation process. It also provides computer simulation results in terms of achievable capacity for BPSK and 2PPM modulation.
- Section 7 provides a description of non–coherent HDF IR–UWB receivers (energy detector and LDR) and demodulation process. Also, it provides computer simulation results of a similar nature to the non–coherent approach.
- Section 8 compares HDF and non–HDF approach to a cooperation communication in terms of its achievable capacity.
- Section 9 concludes the report.

3 Relation of Interference Mitigation/Avoidance (IMA) and Wireless Network Coding (WNC)

3.1 Interference Mitigation vs. WNC

Majority of effort in WP2 is focused on interference mitigation/avoidance (IMA) — all interference between UWB devices and non-UWB/UWB devices is regarded as a harmful phenomena. Dealing with interference as a harmful phenomena comprises several problems — interference classification and identification [3, 7, 8], interference localization and tracking [4], interference mitigation [5] and beamforming/MIMO [6]. However, interference can also be used by WNC principle in order to provide better performance.

The difference between IMA and WNC is as follows. In case of IMA, the communication is in fact a single user communication as seen in conventional communication systems where any other signal present except for the one from the intended transmitter is a harmful interference degrading the performance. Possibility of multiple hops over several nodes is also viable. On the other hand, in WNC, generally, some nodes of the network deal with the intended superposition of signals from several nodes (interference) and perform the decoding in a special manner. They decode so called hierarchical data which are data in fact non existing in the network but representing more data streams given the knowledge of other data streams — e.g. if the hierarchical data are decoded as a symbol–wise modulo addition of two data, it is possible to decode one data given the other data. Nodes decoding hierarchical data from the interference of signals are called relay nodes. There is a possibility of large number of WNC strategies according to the network topology, signal processing, however, in this document we restrict ourselves to two–way relay channel (2WRC) where two end–nodes communicate with each other via intermediate relay node.

3.2 Requirements for WNC

To be able to use WNC, all nodes (devices) are allowed to transmit in the same frequency band, in the same time. They may also use the same signal structure. Also, the network topology must be given which then consequences into the strategy which can be used. It is apparent that, concerning UWB, only the situation when all nodes use UWB enables to use WNC. Any other signal with different structure (e.g. Wi-Fi) or signal from UWB node not present in the intended network topology is unwanted interference degrading the performance.

3.3 Overall Description of WNC in UWB

In this document, we use WNC strategy called Hierarchical decode and forward (HDF) in the aforementioned 2WRC comprising two end–nodes and relay. 2WRC is useful when both end–nodes are not able to communicate with each other directly but intermediate relay node enables

their mutual communication. Considering the situation of transferring one symbol from end–node to end–node and vice versa via relay, using conventional systems, this communication would take four steps. Using HDF, this communication would take two steps which consequences into doubling data rate in case of 2WRC.

4 Description of HDF Strategy

Here we describe all formal details of Hierarchical Decode and Forward (HDF) strategy [14, 15]. Although the principle of this cooperation strategy is generally applicable in more complex scenarios, we assume a two–way relay channel (2WRC) in this document which is depicted in figure 4.1.

This scenario consists of two end nodes, A and B, communicating with each other simultaneously via the intermediate relay node R. Relay node decodes so called hierarchical data representing the intended data at the end nodes given complementary side–information (C–SI) which is a knowledge of the end node's own data. All nodes are assumed to be physically separate and capable of half–duplex communication using IR–UWB only. The process of transferring one symbol from A to B and from B to A takes two phases instead of four phases as it would be in the case of conventional (non–cooperative) systems. These two phases are called Hierarchical MAC phase (H–MAC) and Hierarchical Broadcast phase (H–BC). Since the system is symmetric, we can investigate e.g. a flow of data from A to B and all conclusions are equally applicable to the flow from B to A.

4.1 System Model

4.1.1 H–MAC Phase

We assume that both nodes, A and B, produce data sequences $\mathbf{d_A}$, $\mathbf{d_B}$ composed of data symbols $d_A, d_B \in \mathcal{A}_d = \{0, 1, \ldots, M_d - 1\}$ where $M_d = |\mathcal{A}_d|$ is an alphabet cardinality. Data sequences are encoded into codewords $\mathbf{c_A}$, $\mathbf{c_B}$ composed of codeword symbols $c_A, c_B \in \mathcal{A}_c = \{0, 1, \ldots, M_c - 1\}$ where $M_c = |\mathcal{A}_c|$ is a codeword symbols alphabet cardinality. These codewords are then mapped into signal space point sequences $\mathbf{q_A}$, $\mathbf{q_B}$ using per symbol mapping operation $q = \mathcal{M}(c)$ where $\mathcal{M}(.)$ is a mapping operation. We will use a notation $q_{A,k}$ for the k-th symbol from $\mathbf{q_A}$. We will denote codebooks of A and B as $\mathcal{C}_A$ and $\mathcal{C}_B$, respectively. Let us now describe signals transmitted by the nodes and received at relay in H–MAC phase. We assume a symbol interval consisting of several frames, each carrying one pulse. Neither direct sequence (DS) nor time–hopping (TH) codes are assumed. This simplifies the problem without loss of generality because we assume that only signals from A, B and R are present and if DS or TH

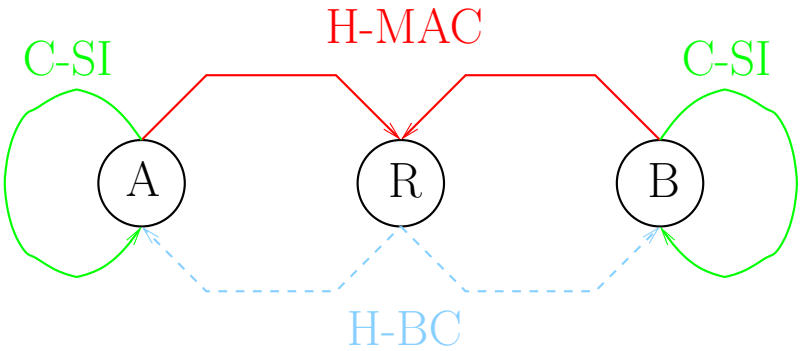

Figure 4.1: Two–way relay channel

codes were present they had to be the same which would not result into different performance. Now we describe signals structure which is in accordance with [19].

4.1.1.1 BPSK

In the case of BPSK modulation, the signal transmitted by node A is

$$s_A(t) = \sum_{k=-\infty}^{\infty} \sum_{l=0}^{N_f-1} q'_{A,k}\, p_t(t - kT_s - lT_f) \tag{4.1}$$

where N_f is a number of pulses per symbol, $p_t(t)$ is a transmitted pulse, T_s is a symbol duration and T_f is a frame duration. Also,

$$q'_{A,k} = \begin{cases} -1 & \text{if} \quad q_{A,k} = 0 \\ 1 & \text{if} \quad q_{A,k} = 1 \end{cases} . \tag{4.2}$$

The effect of UWB channel from A to R can be described by the channel impulse response (CIR) $h_A(t)$. The useful signal from A at R is then $u_A(t) = (s_A * h_A)(t)$ where $*$ stands for a convolution operation. We can write

$$u_A(t) = \sum_{k=-\infty}^{\infty} \sum_{l=0}^{N_f-1} q'_{A,k}\, p_{r,A}(t - kT_s - lT_f) \tag{4.3}$$

where $p_{r,A}(t) = (p_t * h_A)(t)$ is a waveform complying to one pulse from A received at R. The same holds for signals from B — the difference is that the useful signal from B at R is $p_{r,B}(t) = (p_t * h_B)(t)$ where generally $h_A(t) \neq h_B(t)$.

4.1.1.2 NPPM

In the case of NPPM modulation, the signal transmitted by node A is

$$s_A(t) = \sum_{k=-\infty}^{\infty} \sum_{l=0}^{N_f-1} p_t(t - kT_s - lT_f - q_{A,k}\delta) \tag{4.4}$$

N_f is a number of pulses per symbol, $p_t(t)$ is a transmitted pulse, T_s is a symbol duration, T_f is a frame duration and δ is a time separation for different symbols. Again, the useful signal from A at R is

$$u_A(t) = \sum_{k=-\infty}^{\infty} \sum_{l=0}^{N_f-1} p_{r,A}(t - kT_s - lT_f - q_{A,k}\delta) \tag{4.5}$$

where $p_{r,A}(t) = (p_t * h_A)(t)$ is a waveform complying to one pulse from A received at R. The same holds for signals from B — the difference is that the useful signal from B at R is $p_{r,B}(t) = (p_t * h_B)(t)$ where generally $h_A(t) \neq h_B(t)$.

4.1.1.3 Received Signal at R

The signal received at R is

$$x_R(t) = \overbrace{u_A(t) + u_B(t - \Delta)}^{u(t)} + w_R(t) \tag{4.6}$$

where $u_A(t)$ and $u_B(t)$ are given by (4.3) or (4.5) according to the used modulation and Δ is a mutual time–shift of the useful signals from A and B at R which may occur due to the fact that the UWB pulses are very short and time synchronization can be imperfect. Also, $w_R(t)$ in (4.6) is AWGN with double–sided power spectral density (PSD) $N_0/2$. The signal processing at the relay in the H–MAC phase is described in sections 6 and 7 dealing with a coherent and a non–coherent approach respectively.

4.1.2 H–BC Phase

The relay processes the received signal $x_R(t)$ so as to obtain an estimate of a hierarchical data message $\hat{\mathbf{d}}_{\mathbf{AB}}$ fully representing a desired data message at the end node given the knowledge of C–SI. The message $\hat{\mathbf{d}}_{\mathbf{AB}}$ is encoded into a codeword $\mathbf{c_R}$ composed of codeword symbols $c_R \in \mathcal{A}_R = \{0, 1, \ldots, M_R - 1\}$ where $M_R = |\mathcal{A}_R|$ is a relay codeword symbol alphabet cardinality. Message $\mathbf{c_R}$ is then mapped into signal space points message $\mathbf{v}$ which is then broadcast to both A and B and used to obtain the desired data message. We will denote a relay codebook as $\mathcal{C}_R$.

4.1.2.1 BPSK

For BPSK, the signal transmitted by R is

$$s_R(t) = \sum_{k=-\infty}^{\infty} \sum_{l=0}^{N_f-1} v'_{R,k}\, p_t(t - kT_s - lT_f) \tag{4.7}$$

where $v'_{R,k}$ is the k-th symbol in sequence $\mathbf{v}'$ such that

$$v'_{R,k} = \begin{cases} -1 & \text{if} \quad v_{A,k} = 0 \\ 1 & \text{if} \quad v_{A,k} = 1 \end{cases} . \tag{4.8}$$

The useful signal from R at B is

$$u_R(t) = \sum_{k=-\infty}^{\infty} \sum_{l=0}^{N_f-1} v'_{R,k}\, p_{r,R}(t - kT_s - lT_f) \tag{4.9}$$

where $p_{r,R}(t) = (p_t * h_B)(t)$ and we assumed the same channel between B and R in H–BC phase as in H–MAC phase.

4.1.2.2 NPPM

For NPPM, the signal transmitted by R is

$$s_R(t) = \sum_{k=-\infty}^{\infty} \sum_{l=0}^{N_f-1} p_t(t - kT_s - lT_f - v_{R,k}\delta). \tag{4.10}$$

The useful signal from R at B is

$$u_R(t) = \sum_{k=-\infty}^{\infty} \sum_{l=0}^{N_f-1} p_{r,R}(t - kT_s - lT_f - v_{R,k}\delta) \tag{4.11}$$

where $p_{r,R}(t) = (p_t * h_B)(t)$ and we assumed the same channel between B and R in H–BC phase as in H–MAC phase.

4.1.2.3 Received Signal at B

The received signal at B is

$$y_B(t) = u_R(t) + w_B(t) \tag{4.12}$$

where $w_B(t)$ is AWGN with PSD $N_0/2$.

4.2 Hierarchical Exclusive Codebook

Here we describe required and some of the other important properties of the mapping $\mathbf{d_{AB}}(\mathbf{d_A}, \mathbf{d_B})$ which will be than called Hierarchical Exclusive Code (HXC) [14].

4.2.1 Exclusive Law

A mapping $\mathbf{d_{AB}}(\mathbf{d_A}, \mathbf{d_B})$ must fulfil an exclusive law which can be written as

$$\mathbf{v}\left(\mathbf{d_{AB}}(\mathbf{d_A}, \mathbf{d_B})\right) \neq \mathbf{v}\left(\mathbf{d_{AB}}(\mathbf{d'_A}, \mathbf{d_B})\right), \quad \forall \mathbf{d_A} \neq \mathbf{d'_A}, \tag{4.13}$$

$$\mathbf{v}\left(\mathbf{d_{AB}}(\mathbf{d_A}, \mathbf{d_B})\right) \neq \mathbf{v}\left(\mathbf{d_{AB}}(\mathbf{d_A}, \mathbf{d'_B})\right), \quad \forall \mathbf{d_B} \neq \mathbf{d'_B} \tag{4.14}$$

for signal space point sequences and as

$$\mathbf{d_{AB}}(\mathbf{d_A}, \mathbf{d_B}) \neq \mathbf{d_{AB}}(\mathbf{d'_A}, \mathbf{d_B}), \quad \forall \mathbf{d_A} \neq \mathbf{d'_A}, \tag{4.15}$$

$$\mathbf{d_{AB}}(\mathbf{d_A}, \mathbf{d_B}) \neq \mathbf{d_{AB}}(\mathbf{d_A}, \mathbf{d'_B}), \quad \forall \mathbf{d_B} \neq \mathbf{d'_B} \tag{4.16}$$

for data sequences. Equations (4.15) and (4.16), or (4.13) and (4.14), guarantee an invertibility of the mapping $\mathbf{d_{AB}}(\mathbf{d_A}, \mathbf{d_B})$ allowing the end nodes to obtain the data intended to them from the hierarchical data given the knowledge of C–SI. Let us note that conditions (4.15) and (4.16) must be fulfilled in every part of the system.

A code satisfying conditions (4.13) and (4.14) will be called Hierarchical Exclusive Code (HXC).

4.2.2 Relay Hierarchical Codebook Cardinality

We can see that $\max(|\mathcal{C}_A|, |\mathcal{C}_B|) \leq |\mathcal{C}_R| \leq |\mathcal{C}_A||\mathcal{C}_B|$ where $|\mathcal{C}_A|$, $|\mathcal{C}_B|$, $|\mathcal{C}_R|$ denote codebooks cardinality. A mapping satisfying $\max(|\mathcal{C}_A|, |\mathcal{C}_B|) = |\mathcal{C}_R|$ is called a minimal mapping. The name stems from the fact that $|\mathcal{C}_R|$ is in such a case minimal while satisfying an exclusive law (invertibility of the mapping). All other mappings with $\mathcal{C}_R$ greater than minimal will be called extended. The opposite case to the minimal mapping is a mapping satisfying $|\mathcal{C}_R| = |\mathcal{C}_A||\mathcal{C}_B|$ which is in fact a joint decoding as in the classical MAC channel.

4.2.3 Layered Hierarchical Design for a Minimal Mapping

A direct design of a mapping $\mathbf{v}\left(\mathbf{d_{AB}}(\mathbf{d_A}, \mathbf{d_B})\right)$ can be very complex. A way how to simplify the problem is to divide the mapping into two layers — the outer layer can be an error correcting code (e.g. a state-of-the-art capacity achieving code) while the inner layer provides an exclusive property. The simplest example of the inner layer is a per symbol mapper

$$c_{AB} = \mathcal{X}_c(c_A, c_B) \tag{4.17}$$

fulfilling the exclusive law. This mapper is called a Hierarchical eXclusive Alphabet (HXA). This approach allows us to simply obtain a metric for codeword symbols on a per symbol basis

which can be then used to decode the codeword $\mathbf{c_{AB}}$ yielding $\mathbf{d_{AB}}$. Requirements of HXA are fulfilled if the mapping $c_{AB} = \mathcal{X}_c(c_A, c_B)$ is e.g. $c_{AB} = c_A + c_B \bmod M_c$ or a bit–wise XOR operation over c_A and c_B.

4.3 Decoding at Relay

4.3.1 Decoding at Relay using a Coherent Approach

If the receiver at R is a coherent type of receiver (matched filter), the receiver at R obtains a signal space point x_n for every symbol interval. This allows us to obtain a likelihood for a hierarchical codeword symbol. Let us assume a minimal mapping $\mathcal{X}_c(.,.)$ and let us drop sequence indices for simplicity. Since the received signal is given by codeword symbols from A and B but we are interested in likelihood for a hierarchical symbol, we can write

$$\begin{aligned} p(x|c_{AB}) &= p\left(x|\cup_{c_A,c_B:\mathcal{X}_c(c_A,c_B)=c_{AB}}\{c_A,c_B\}\right) \\ &= \frac{p\left(x\cap\left(\cup_{c_A,c_B:\mathcal{X}_c(c_A,c_B)=c_{AB}}\{c_A,c_B\}\right)\right)}{p\left(\cup_{c_A,c_B:\mathcal{X}_c(c_A,c_B)=c_{AB}}\{c_A,c_B\}\right)}. \end{aligned} \tag{4.18}$$

Since the pairs $\{c_A, c_B\}$ are disjoint, we can write

$$p(x|c_{AB}) = \frac{\sum_{c_A,c_B:\mathcal{X}_c(c_A,c_B)=c_{AB}} p(x|c_A,c_B)\,p(c_A,c_B)}{\sum_{c_A,c_B:\mathcal{X}_c(c_A,c_B)=c_{AB}} p(c_A,c_B)}. \tag{4.19}$$

We assume that c_A and c_B are independent and identically distributed (i.i.d.), thus pairs (c_A, c_B) are i.i.d. too. We can then write

$$p(x|c_{AB}) = \frac{\sum_{c_A,c_B:\mathcal{X}_c(c_A,c_B)=c_{AB}} p(x|c_A,c_B)}{M_c} \tag{4.20}$$

where $M_c = \sum_{c_A,c_B:\mathcal{X}_c(c_A,c_B)=c_{AB}} 1$.

Having obtained a likelihood $p(x|c_{AB})$, we can compute a capacity of the system according to the following formula

$$C = I(c_{AB}; x) = H(x) - H(x|c_{AB}). \tag{4.21}$$

where $I(X;Y)$ denotes a mutual informatino between random variables X and Y and $H(X)$ is an entropy of a random variable X. We note that C in (4.21) is, in fact, not a capacity as it is usually understood (e.g. in [2]). Here, we do not perform a maximization over input distribution and so C in (4.21) is an alphabet constrained capacity.

4.3.2 Decoding at Relay using a Non–Coherent Approach

If the receiver at R is a non–coherent receiver, we assume an energy detector (ED) for a full–resolution receiver ([13]) and we also investigate an applicability of HDF in case of Low data rate platform (LDR) which uses a received signal quantization. For either type of non–coherent receiver, the receiver observes the received signal complying to $c_{AB,k}$ through one decision variable $i_{BPSK}[k]$ for BPSK and a set of decision variables $\left\{i^{(0)}_{NPPM}[k],\ldots,i^{(N-1)}_{NPPM}[k]\right\}$ for NPPM. We will investigate an applicability of binary modulations (BPSK and 2PPM) for a non–coherent receiver. The receiver performs a decision, or a set of decisions, over decision variable, or variables, based upon an appropriately set threshold T_o. Given a general threshold T, we can compute the transition probabilities

$$p_{mn}(T) = p(\hat{c}_{AB} = n|c_{AB} = m, T) \tag{4.22}$$

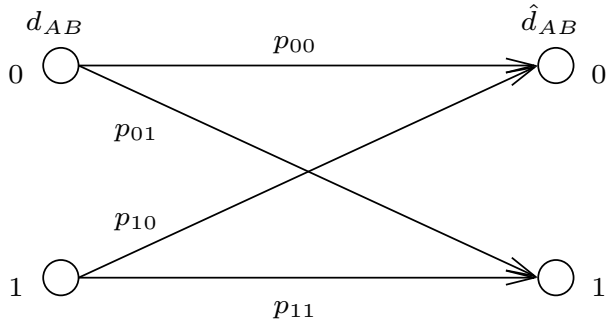

Figure 4.2: Binary channel

where $\hat{c}_{AB}$ is an estimate of c_{AB} at R. Having the transition probabilities, we can transform whole problem into a binary channel depicted in figure 4.2.

We can then compute an alphabet constrained capacity of the binary channel as follows

$$C(T) = H\left(\hat{c}_{AB}|T\right) - H\left(\hat{c}_{AB}|c_{AB}, T\right). \tag{4.23}$$

Since we use a binary alphabet of c_{AB} we can simplify a whole derivation by using a function $H_p(x) = -x\log_2 x - (1-x)\log_2(1-x)$, as in [2]. Then we can write

$$H(\hat{c}_{AB}|T) = H_p\left(p(\hat{c}_{AB} = 0|T)\right) = H_p\left(\frac{1}{2}p_{00}(T) + \frac{1}{2}p_{10}(T)\right) \tag{4.24}$$

where we used i.i.d. assumption of c_{AB} and

$$H(\hat{c}_{AB}|c_{AB}, T) = \sum_{i=0}^{1} p(c_{AB} = i)\, H(\hat{c}_{AB}|c_{AB} = i, T) = \frac{1}{2}H_p(p_{01}) + \frac{1}{2}H_p(p_{10}). \tag{4.25}$$

For a given combination of $h_A(t)$ and $h_B(t)$, an optimal threshold T_o is set in order to maximize $C(T)$ yielding $C = C(T_o)$.

5 UWB Technology

5.1 UWB Technology

Any wireless communication technology occupying a bandwidth larger than some given value can be called an Ultra-Wideband technology. This limit is given by the local regulatory body. In the case of the European Union the regulator is the European Commission. The mandatory condition for the UWB technology can be found in [1].

There are two principal ways how to occupy the sufficient amount of the frequency spectrum. The first one is an Impulse Radio UWB (IR–UWB). The huge bandwidth is achieved by transmission of very short (in nanosecond or even sub-nanosecond) pulse. The second way is a multi-carrier technique based on the OFDM technology [11]. In this report we will assume the first mentioned method – the IR-UWB – because it opens novel specifics and issues.

UWB technology is mainly aimed for short range and high data rate applications. The UWB equipment has a possibility to be simple and low power demanding which makes the UWB to be an attractive technology for various applications like cable replacement, Wireless USB, sensor networks, wireless distribution of entertainment for indoor, automotive or aircraft environments [19].

5.2 UWB Indoor Propagation

Due to the huge occupied bandwidth the UWB exhibits a very specific propagation behavior especially in the indoor environment. The indoor environment inherently introduces a multipath propagation. The transmitted electromagnetic waves travel through the environment, interact with the objects and after some time arrive to the receiver antenna where they are summed up. Due to the different path and different interactions every multipath component is affected differently. The received signal is thus a sum of components with various delays and attenuations.

The mutual position of transmitter, receiver and neighboring objects can vary with time which causes the amplitudes and delays of the multipath components become random variables. But the channel is usually assumed to be constant over given time portion, e.g. to be block constant.

The distribution of objects in a typical indoor environment is not the uniform one. The objects are usually grouped together. They form clusters. It is obvious that the multipath components have to be grouped together in clusters too. The reflection from one cluster of objects will happen almost in one time instant with similar properties. Hence the delays and the amplitudes of all multipath components reflected from given cluster of objects will be correlated. The popular channel model which represents all of behavior presented herein is a Saleh-Valenzuela (SV) channel model. This channel model was adopted by IEEE P802.15 Working Group for Wireless Personal Area Networks in the report [10].

The channel model is mathematically described by

$$h(t) = X \sum_{l=0}^{L} \sum_{k=0}^{K} \alpha_{k,l} \delta(t - T_l - \tau_{k,l}) \tag{5.1}$$

where $\alpha_{k,l}$ are the multipath gain coefficients, T_l is the arrival time of the l-th cluster, $\tau_{k,l}$ is

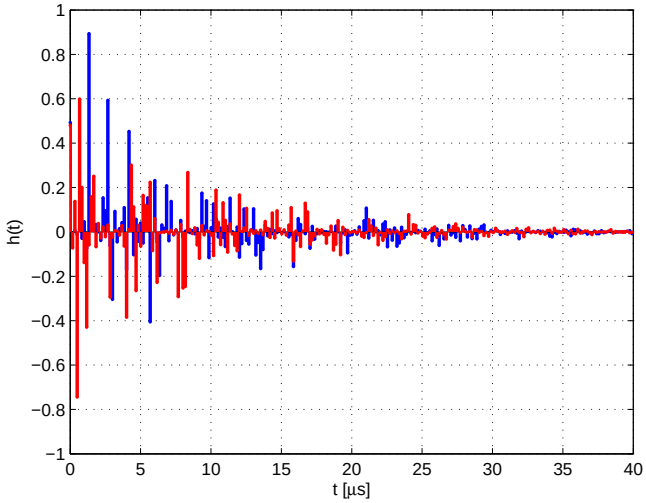

Figure 5.1: Channel impulse response

the delay of the k-th multipath component relatively to the l-th cluster arrival time and X represents the log-normal shadowing, $\delta(t)$ denotes the Dirac delta function.

Parameters of individual random variables depend on the concrete channel model. The report [10] provides four basic models CM1–CM4 with different parameters for various indoor environments. The applicable range as well as the presence or absence of the line-of-sight (LOS) component determines the channel properties. Properties of the individual models are in the following list:

- CM1 — range up to 4 meters, LOS,
- CM2 — range up to 4 meters, NLOS,
- CM3 — range from 4 to 10 meters, NLOS,
- CM4 — 25ns RMS delay, NLOS.

The number of resolvable multipath components depends on concrete model, but is generally high, from tens to even more than one hundred. This makes the optimal receivers, such as RAKE, very complex.

Fig. 5.1 shows two random realizations of the channel impulse response (CIR) according to CM1.

5.3 UWB Receivers

The UWB receivers can be generally divided into two main groups. The first one utilize the optimal receiver structures for the narrowband communications and extends it to the UWB. This leads to a RAKE receiver. Although this is the optimal solution it has a lot of drawbacks. Firstly, the fully digital receiver must be able to provide a correct sampling i.e. at least at the Nyquist frequency. The only practically possible implementation for such a high rates as in the UWB is an analog-to-digital conversion done in parallel. This makes the receiver very complex and power demanding. Secondly, for an optimal collection of satisfactory amount of the energy in the multipath environment the RAKE receiver must utilize a large number of fingers. All of these properties make the RAKE receiver to be very complex.

Since the UWB technology is aimed to be low-cost and low-power the simple receiver structures are necessary. This leads to the second group of the UWB receiver structures. These are energy detectors or autocorrelation receivers. Although such a receiver will by a simple one the price that must be paid is its suboptimality. Suboptimal receiver structures will inherently need higher SNR to achieve the same properties (e.g. BER) as the optimal one [18].

6 Coherent Approach

6.1 Receiver with the Subspace Projection

In this chapter we will provide the description of the coherent approach to the UWB detection. By the term "coherent" we mean that the receiver has knowledge – full or even only partial – about the channel impulse response.

We will assume a receiver with the projection to given subspace at its input. The main idea of this structure is to decrease the complexity of the received signal. Each symbol is represented by one N dimensional vector instead of the signal shape in time domain. This allows us to use the "constellation" space description with useful analysis of the minimal distance which determines the performance of the system. The second useful fact is that by various choices of the subspaces we can assume the trade-off between the receiver complexity and its performance.

In this chapter we provide formal description of the receiver structure, mathematical description of the projection, the way how to represent received signal in terms of the constellation space. All of these results are numerically evaluated to obtain the MAC capacity as a function of SNR for various channel realizations. We also evaluate a BER for this system model.

We still assume the 2WRC network topology. All other of our assumptions are in agreement with the definitions in Chapter 4.

6.1.1 Receiver Model

Receiver structure is depicted on Fig. 6.1. Incoming signal is a superposition of all (in our case 2) transmitted useful signal and of the AWGN.

Useful part is given by

$$u(t) = u_A(t) + u_B(t) \tag{6.1}$$

where individual useful signals $u_A(t), u_B(t)$ depend on the used modulation – for BPSK given by (4.3) and for 2PPM by (4.5).

This signal is at the input of the receiver projected into the given subspace. The formal details on this projection will be described in the following section. As a result of the projection receiver obtain a constellation space N dimensional vector $\mathbf{x}$ per each symbol. Form this vector the soft-output demodulator $\mathcal{M}_{AB}$ produces symbol-wise metric $\mu(c_{AB})$ on hierarchical symbols c_{AB}, e.g. likelihoods. Based on this metric the decoder $\mathcal{D}_{AB}$ produces the estimates of transmitted hierarchical symbols $\hat{d}_{AB}$.

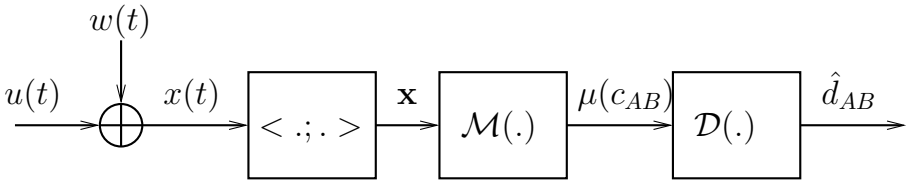

Figure 6.1: Receiver with the subspace projection

6.1.2 Projection Principle

Now we will state formal assumptions on the projection subspace. The subspace is defined by the set of N basis functions $\xi_i(t)$ – i.e. $\{\xi_i(t)\}_{i=1}^{N}$. These functions are assumed to by mutually orthonormal.

In this chapter we will assume N-ary Pulse Position Modulation (NPPM). The signal corresponding to one transmitted symbol may consist of several frames with one pulse transmitted in each. For simplicity we will assume one frame per one symbol. Each frame consist of N consecutive PPM time slots. The pulse shape is transmitted in exactly one of them according to the data. The length of the time slot is assumed to be significantly higher then the rms delay spread of the channel. Thus we avoid the interferences between the pulses.

Under the assumption of NPPM we can simplify the choice of the set of basis functions in the following way. We will assume the $\xi_i(t)$ to have the same form for every i. The i-th function is assumed to be nonzero only within the i-th time slot. Thus we have N same shaped functions properly shifted in time to have one function per each time slot. This obviously form the orthogonal set and under the assumption that $||\xi_i(t)||^2 = 1$ for every i we have got the orthonormal set of functions. Note that the number of functions corresponds to the cardinality of the source PPM alphabet.

Projection of the received signal into the given subspace is described by properly defined the inner scalar product $\langle \cdot ; \cdot \rangle$. Projection of the useful signal into the subspace corresponding to the i-th time slot is given by

$$\begin{aligned} u_i &= \langle u(t); \xi_i(t) \rangle = \\ &= \langle (h_A * s_A)(t) + (h_B * s_B)(t); \xi_i(t) \rangle = \\ &= \langle (h_A * s_A)(t); \xi_i(t) \rangle + \langle (h_B * s_B)(t); \xi_i(t) \rangle \end{aligned} \tag{6.2}$$

where $(\cdot * \cdot)(t)$ denotes convolution, $h_A(t), h_B(t)$ are respective channel impulse responses and $s_A(t), s_B(t)$ are transmitted signals from the sources.

The assumption of the PPM modulation and the choice of the subspace described herein also gives us

$$\langle (h_A * s_A)(t); \xi_i(t) \rangle = \int (h_A * s_A)(t) \xi_i(t) \mathrm{d}t = \begin{cases} \int (h_A * s_A)(t) p(t) \mathrm{d}t & \text{if p(t) is in slot} \\ 0 & \text{elsewhere} \end{cases} \tag{6.3}$$

We will denote the projection of the time slot with the transmitted pulse for source SA by $\alpha = \int (h_A * s_A)(t) p(t) \mathrm{d}t$ and similarly for the source SB by $\beta = \int (h_B * s_B)(t) p(t) \mathrm{d}t$.

Having all of these definitions we can group all of the projection into the N dimensional vector $\mathbf{u}$. Signal space representation of transmitted symbols $\mathbf{c}_A, \mathbf{c}_B$ can be used as an indicator of position of α respectively β. Due to the properties of UWB we can restrict to real vectors i.e. $\mathbf{u} \in \mathbb{R}^N$.

$$\mathbf{u} = \begin{pmatrix} u_1 \\ \vdots \\ u_N \end{pmatrix} = \alpha \mathbf{c}_A + \beta \mathbf{c}_B \tag{6.4}$$

Concretely for 2PPM modulation we obtain 4 results according the transmitted data

$$\mathbf{u} = \begin{pmatrix} u_1 \\ u_2 \end{pmatrix} = \begin{cases} \alpha \begin{pmatrix} 1 \\ 0 \end{pmatrix} + \beta \begin{pmatrix} 1 \\ 0 \end{pmatrix} = \begin{pmatrix} \alpha+\beta \\ 0 \end{pmatrix} \\ \alpha \begin{pmatrix} 1 \\ 0 \end{pmatrix} + \beta \begin{pmatrix} 0 \\ 1 \end{pmatrix} = \begin{pmatrix} \alpha \\ \beta \end{pmatrix} \\ \alpha \begin{pmatrix} 0 \\ 1 \end{pmatrix} + \beta \begin{pmatrix} 1 \\ 0 \end{pmatrix} = \begin{pmatrix} \beta \\ \alpha \end{pmatrix} \\ \alpha \begin{pmatrix} 0 \\ 1 \end{pmatrix} + \beta \begin{pmatrix} 0 \\ 1 \end{pmatrix} = \begin{pmatrix} 0 \\ \alpha+\beta \end{pmatrix} \end{cases} \tag{6.5}$$

At the relay receiver an AWGN is added to the useful signal. The noisy received signal is

$$\mathbf{x} = \mathbf{u} + \mathbf{w} = \alpha \mathbf{c}_A + \beta \mathbf{c}_B + \mathbf{w} \tag{6.6}$$

where $\mathbf{w}$ is N dimensional real valued AWGN vector with variance σ_w^2 per dimension.

Fig. 6.2 shows the constellation of 2PPM modulation according to (6.5) for $\alpha > \beta > 0$. Colored areas on the background of the figures are different decision regions while we assume the bit-wise XOR minimal HXC. Similarly to the narrowband case the parameters α, β can be seen as an UWB channel parameterization. The channel parameterization is shown in [17] to have the significant impact on the capacity of the narrowband system. Some values of the parameterization cause the violence of the exclusive law which leads to a very bad performance

The parameters α, β in the case of the UWB have got an influence on the minimum distance properties of hierarchical constellation which is related to the capacity of the channel. From Fig. 6.2 we can see that the minimal distance d_{min} between the pair of constellation points that have to be distinguished depends on β. For different mutual ratios of α, β we can generalize that $d_{min} \approx \min(|\alpha|, |\beta|)$. Size of the channel parameterization depends on the concrete channel realization as well as on the choice of the subspace for the projection. It shows how much energy is contained in the received signal in the given subspace. This gives us a possibility of optimization of the subspace for the projection taking the channel impulse response into the account.

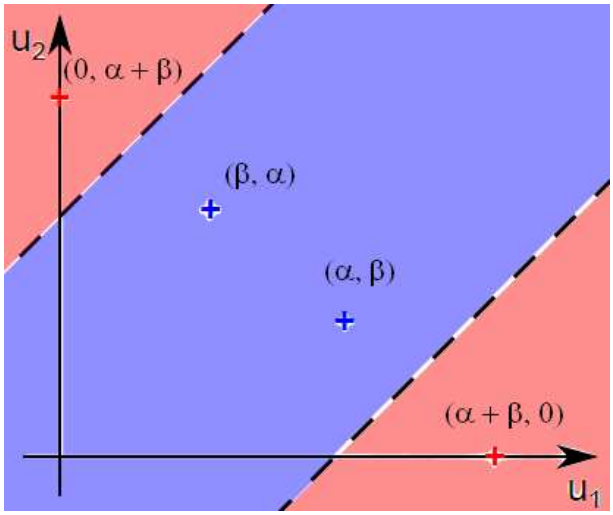

Figure 6.2: Constellation of 2PPM for $\alpha > \beta > 0$

6.1.3 Capacity Evaluation

Evaluation of the MAC capacity proceeds according to the mathematical apparatus presented in Section 4.3.1. We work with the output of the projection – vector $\mathbf{x}$. We evaluate likelihoods for every hierarchical symbol and compute the MAC stage capacity according to (4.21). Details about the numerical simulation can be found in [12, 16].

To illustrate the impact of the various choice of the subspace we evaluate the MAC capacity for two subspaces.

- Subspace of the superposition – $((h_A + h_B) * p)(t)$ – denoted as a composite signal
- Subspace of the transmitted pulse – $p(t)$

The first one is the subspace defined by the transmitted signal when both sources transmit within the same time slot. This subspace obviously needs the perfect knowledge of the channel impulse responses. Thus this will lead to the complex receiver structure. The second subspace is the subspace of the transmitted pulse $p(t)$ at the beginning of the time slot. This subspace has no demands on the knowledge of the channel state. On the other hand is obviously very suboptimal. The system performance will suffer if the channel spread a lot of energy from the beginning of the time slot. The similar performance degradation will happen if the source transmissions will be unsynchronized.

We evaluate the MAC capacity as a function of SNR of 2-WRC network with both of presented subspaces for 2PPM and 4PPM modulation. For comparison we also evaluate the true alphabet unconstrained channel capacity – depicted by black dash-and-dot line in all of the following figures.

Figs. 6.3 and 6.4 show the capacity for 2PPM and 4PPM, respectively, with the composite signal subspace. Curves are parametrized by various channel realization expressed in the terms of $\min(|\alpha|, |\beta|)$. We explicitly plot the maximum (by green line), the minimum (by red line) and the average capacity (by blue line) curves from the given set of randomly generated channel realizations. This colour convention in the legend will be adhered through the rest of this chapter. Note that the distribution between the minimal and the maximal capacity is not the uniform one but follows the properties of the set of the CIRs. Histogram of $|\alpha|$ for composite signal subspace of our test set is depicted on Fig. 6.5. Note that for the composite signal $|\alpha| = |\beta|$.

Figs. 6.6 and 6.7 show the capacity for 2PPM and 4PPM, respectively, with the pulse subspace. The distribution between the minimal and the maximal capacity is now according to the histogram depicted on Fig.6.8. If we compare these results with the results for the composite signal subspace the suboptimality of the transmitted pulse subspace. For some channel realizations its performance is catastrophic (see the red lines). In this case only a very small amount of the energy is usefully collected by the receiver. On the other hand for some channel this subspace works quiet good.

If we compare both histograms, depicted on 6.5 and 6.8. We can see that the values close to zero (which lead to the low capacity) are much more probable for the pulse subspace this again shows the suboptimality of this choice. But the pulse subspace needs no knowledge of the channel impulse response.

Figs. 6.9 and 6.10 show the comparison of the HDF strategy and the Joint Decode and Forward (JDF) strategy, when the relay makes the decision about all individual incoming data streams, for 2PPM modulation. To simplify the situation we assume the same channels between $SA \to R$ and $SB \to R$, i.e. $\alpha = \beta$, as well as the same rate of both users. We assume the same channel realization for both subspaces. Capacity of JDF is given by the first and the second order alphabet limited cut set bounds. The MAC capacity for HDF is depicted in red, the JDF cut set bound capacities by dashed and solid green line. Figs. 6.11 and6.12 show the same

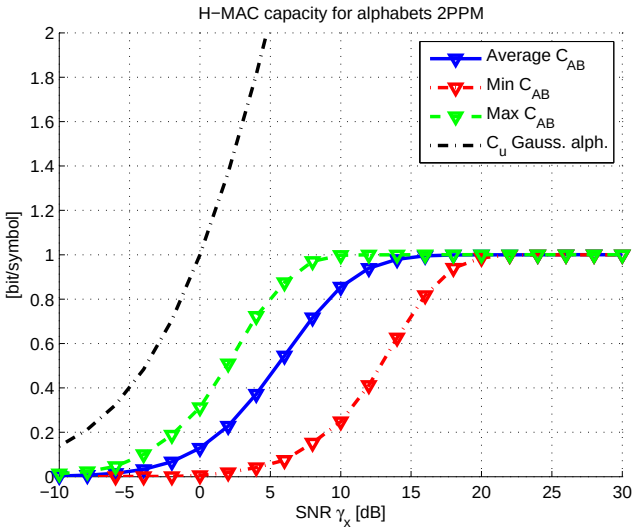

Figure 6.3: H-MAC capacity – 2PPM, composite signal subspace

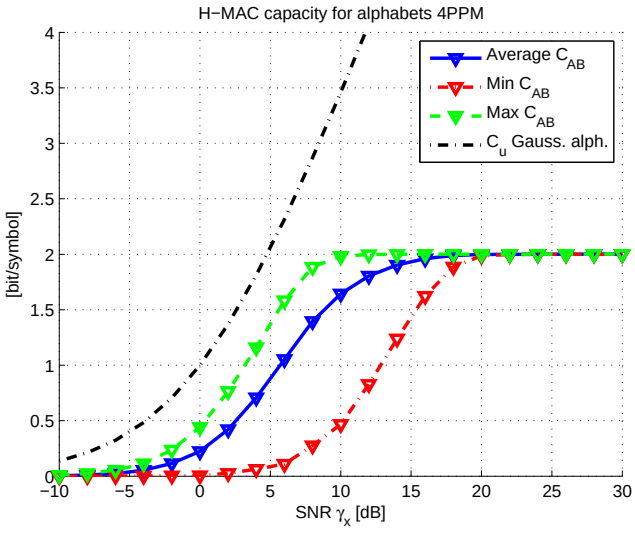

Figure 6.4: H-MAC capacity – 4PPM, composite signal subspace

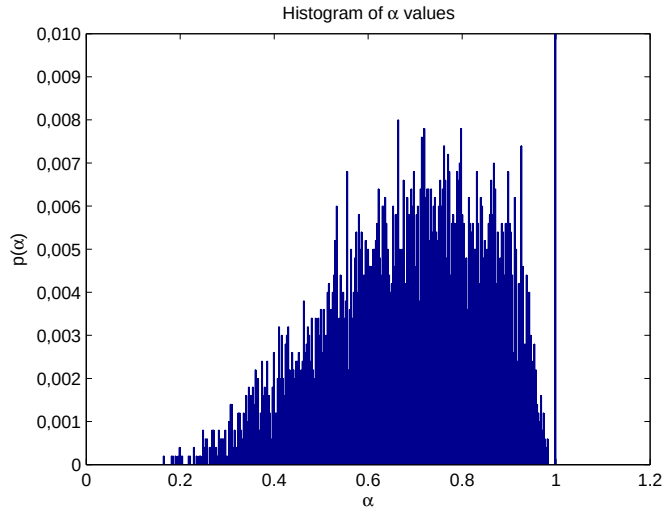

Figure 6.5: Histogram of $\min(|\alpha|, |\beta|)$ – composite signal subspace

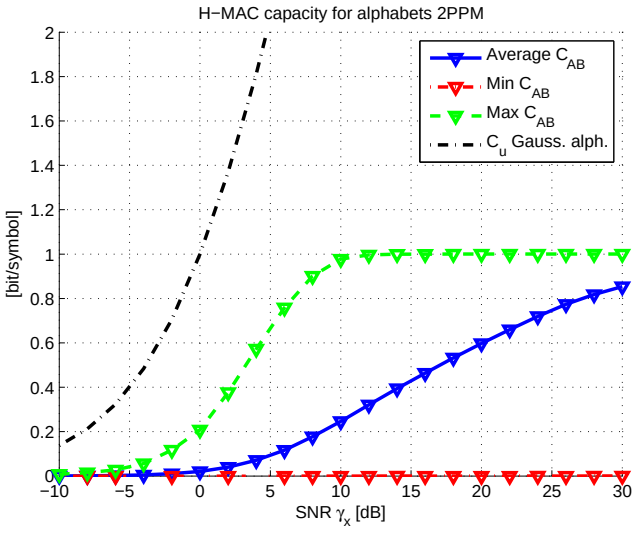

Figure 6.6: H-MAC capacity – 2PPM, pulse subspace

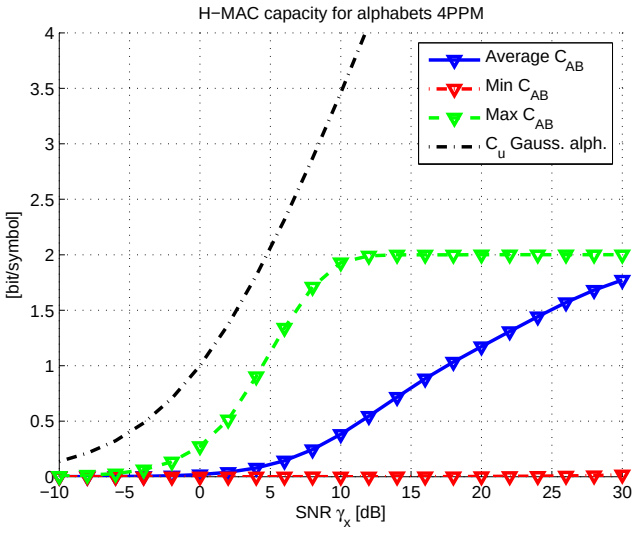

Figure 6.7: H-MAC capacity – 4PPM, pulse subspace

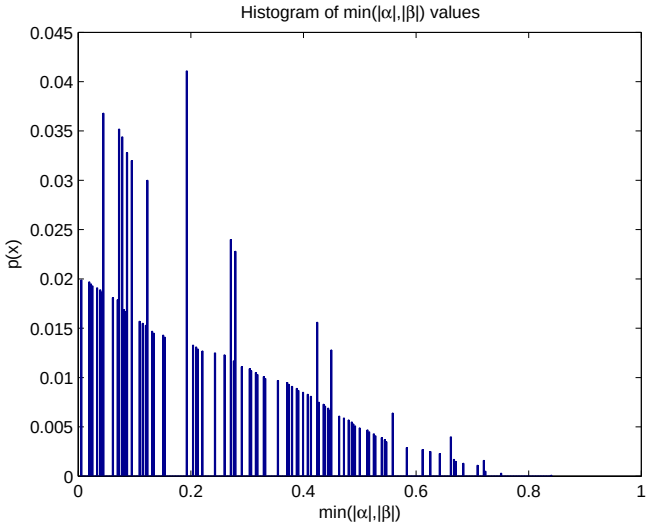

Figure 6.8: Histogram of $\min(|\alpha|, |\beta|)$ – pulse subspace

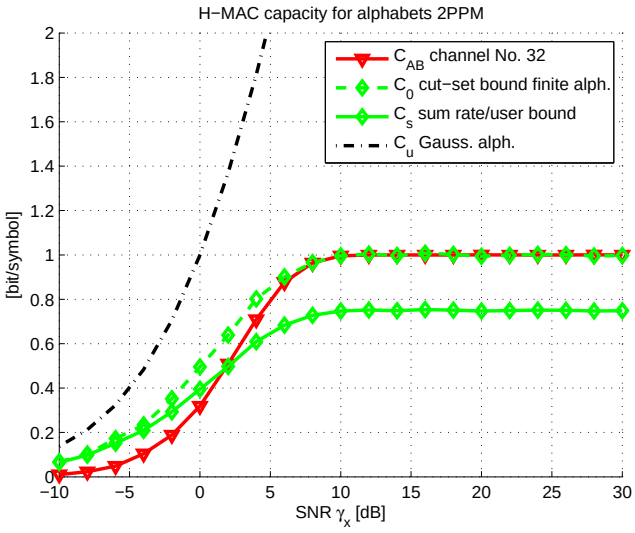

Figure 6.9: H-MAC capacity – HDF vs. JDF – 2PPM, composite signal subspace

comparison for 4PPM modulation. If we compare the results for the same modulation with different used subspace we again see the advantage of the composite signal subspace.

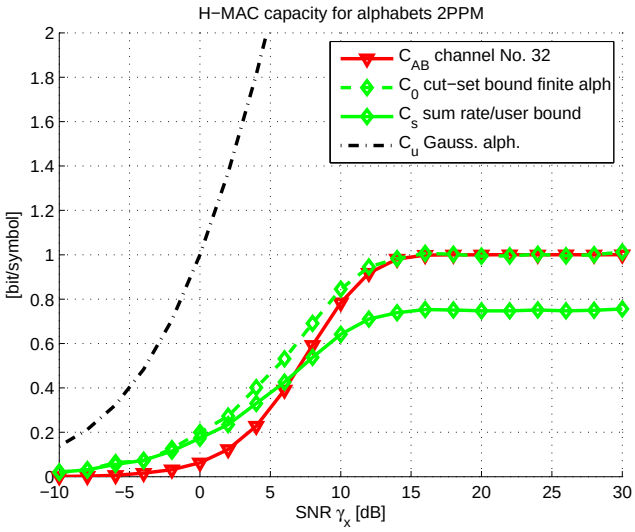

Figure 6.10: H-MAC capacity – HDF vs. JDF – 2PPM, pulse subspace

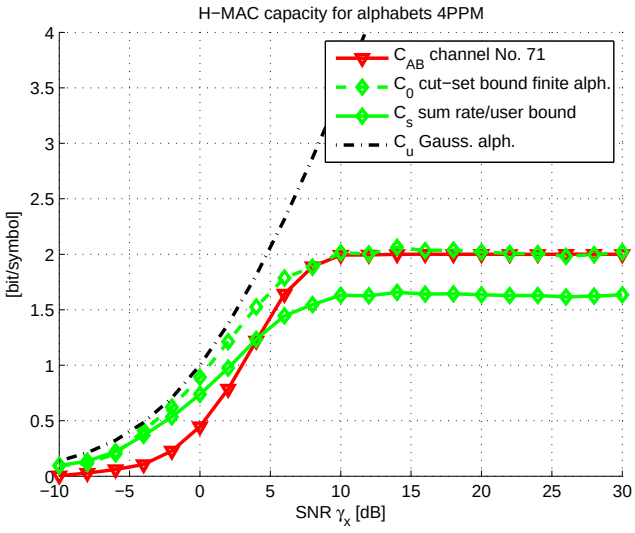

Figure 6.11: H-MAC capacity – HDF vs. JDF – 4PPM, composite signal subspace

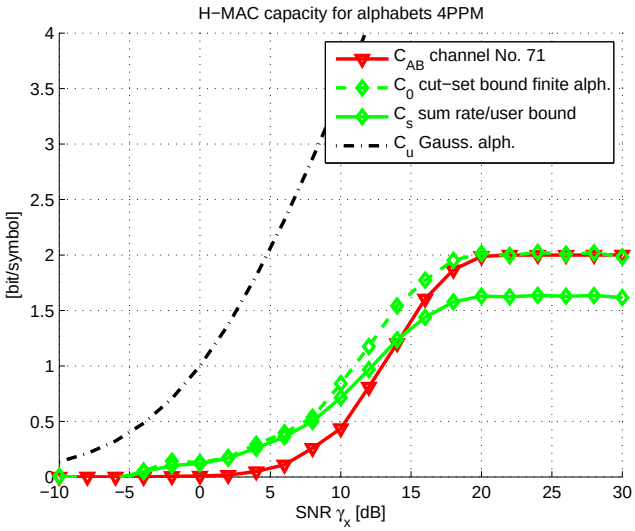

Figure 6.12: H-MAC capacity – HDF vs. JDF – 4PPM, pulse subspace

7 Non–Coherent Approach

7.1 Energy Detector Integration Receiver

7.1.1 Receiver Structure

We assume a full–resolution (in terms of a signal quantization) non–coherent energy detector receiver ([18, 19]), as depicted in figure 7.1. The received signal $x_R(t)$ is first filtered by a bandpass filter, yielding $x_{R,f}(t)$. Than, a squaring operation and an integration over N_f frames complying to the k-th symbol is performed, denoted as $\sum \circ \int \circ()^2$ in the figure suggesting that it is performed as a sum of integrals. For BPSK, this integration yields a decision variable $i_{BPSK}[k]$. For 2PPM, this integration is performed over two sets of time–windows complying to two possible positions of pulses; this yields decision variables $i^{(0)}_{2PPM}[k]$ for a zero time–shift and $i^{(1)}_{2PPM}[k]$ for a time–shift δ in (4.4). Decision block (DEC) then provides an estimate of codeword symbols c_{AB} — $\hat{c}_{AB}$.

Let us note that we assume symbols and frames energetically independent — useful signals from individual frames do not overlap in the received signal.

Let us note that the relay receiver uses the mapping captured in the table 7.1.

7.1.2 BPSK

7.1.2.1 Decision Variable

For k-th symbol, the decision variable is

$$i_{BPSK}[k] = \sum_{l=0}^{N_f-1} \int_{kT_s+lT_f}^{kT_s+lT_f+T_I} x^2_{R,f}(t)\,\mathrm{d}t \tag{7.1}$$

where T_I is an integration interval which is generally not set to capture energy of whole useful signal in order to optimize signal to noise ratio as is dealt with in [18]. We simplify a notation by introducing

$$\mathcal{I}\left(a(t)\right)_k = \sum_{l=0}^{N_f-1} \int_{kT_s+lT_f}^{kT_s+lT_f+T_I} a(t)\,\mathrm{d}t. \tag{7.2}$$

Then

$$i_{BPSK}[k] = \mathcal{I}\left(\left(u(t)+w(t)\right)^2\right)_k = \overbrace{\mathcal{I}\left(u^2_f(t)\right)_k}^{E_k} + \overbrace{\mathcal{I}\left(2u_f(t)\,w_{R,f}(t)\right)_k}^{\zeta_k} + \overbrace{\mathcal{I}\left(w^2_{R,f}(t)\right)_k}^{\eta_k} \tag{7.3}$$

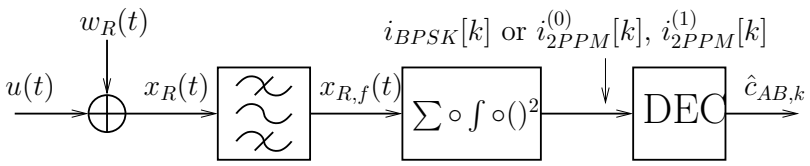

Figure 7.1: Non–coherent receiver structure

	$d_B = 0$	$d_B = 1$
$d_A = 0$	0	1
$d_A = 1$	1	0

Table 7.1: Mapping considered for the non–coherent relay receiver

where E_k is a useful signal energy of the k-th symbol, ζ_k is a zero mean Gaussian noise and η_k is a non–zero mean noise, generally non–Gaussian (see [18]). Also, $u_f(t)$ and $w_{R,f}(t)$ denote a filtered versions of $u(t)$ and $w_R(t)$ respectively. Further, E_k can be expressed as

$$E_k = \mathcal{I}_k\left(u_f^2(t)\right)_k = \overbrace{\mathcal{I}\left(u_{A,f}^2(t)\right)_k}^{E_{A,k}} + \overbrace{\mathcal{I}\left(u_{B,f}^2(t)\right)_k}^{E_{B,k}} + 2q'_{A,k}q'_{B,k}\overbrace{\mathcal{I}\left(u_{A,f}(t)u_{B,f}(t)\right)_k}^{E_{m,k}} \tag{7.4}$$

where $E_{A,k}$ is an energy of the useful signal from A, similarly for B and $E_{m,k}$ is a mutual energy of the useful signals from A and B complying to the case when $q'_{A,k} = q'_{B,k}$. We note that $-\sqrt{E_{A,k}E_{B,k}} \leq E_{m,k} \leq \sqrt{E_{A,k}E_{B,k}}$.

7.1.2.2 Demodulation

We can see from (7.3) and (7.4) that the decision variable $i_{BPSK}[k]$ depends on $c_{A,k}$ and $c_{B,k}$ through $E_{m,k}$. This means that for $q'_{A,k} = q'_{B,k}$ ($c_{AB,k} = 0$ according to the table 7.1) we obtain $i_{BPSK}[k] = E_{A,k} + E_{B,k} + q'_{A,k}q'_{B,k}E_{m,k} + \zeta_k + \eta_k$ while for $q'_{A,k} \neq q'_{B,k}$ we obtain $i_{BPSK}[k] = E_{A,k} + E_{B,k} - q'_{A,k}q'_{B,k}E_{m,k} + \zeta_k + \eta_k$ and so

$$\hat{c}_{AB,k} = \begin{cases} 0; & i_{BPSK}[k] \gtrless T_o \quad \text{for} \quad E_{m,k} \gtreqless 0 \\ 1; & i_{BPSK}[k] \lesseqgtr T_o \quad \text{for} \quad \mathrm{E_{m,k}} \gtreqless 0 \end{cases} \tag{7.5}$$

where T_o is an optimal threshold set so as to maximize the capacity. Probabilities p_{00}, p_{01}, p_{10} and p_{11} can then be obtained from (7.5) with the knowledge of PDF of ζ_k and η_k as follows

$$p_{00} = p\left(i_{BPSK} \gtrless T_o | c_{AB} = 0\right) \quad \text{for} \quad \mathrm{E_m} \gtreqless 0, \tag{7.6}$$

$$p_{01} = p\left(i_{BPSK} \lesseqgtr T_o | c_{AB} = 0\right) \quad \text{for} \quad \mathrm{E_m} \gtreqless 0, \tag{7.7}$$

$$p_{10} = p\left(i_{BPSK} \gtrless T_o | c_{AB} = 1\right) \quad \text{for} \quad \mathrm{E_m} \gtreqless 0, \tag{7.8}$$

$$p_{11} = p\left(i_{BPSK} \lesseqgtr T_o | c_{AB} = 1\right) \quad \text{for} \quad \mathrm{E_m} \gtreqless 0. \tag{7.9}$$

Dependence of $i_{BPSK}[k]$ on $E_{m,k}$ brings also a dependence on channel parametrization — particular combinations of $h_A(t)$ and $h_B(t)$.

7.1.3 2PPM

7.1.3.1 Decision Variables

In order to simplify a notation, we define

$$\mathcal{I}\left(a(t)\right)_k^{(0)} = \sum_{l=0}^{N_f-1} \int_{kT_s+lT_f}^{kT_s+lT_f+T_I} a(t)\,\mathrm{d}t, \tag{7.10}$$

$$\mathcal{I}\left(a(t)\right)_k^{(1)} = \sum_{l=0}^{N_f-1} \int_{kT_s+lT_f+\delta}^{kT_s+lT_f+\delta+T_I} a(t)\,\mathrm{d}t. \tag{7.11}$$

The decision variables for the k-th symbol are then

$$i_{2PPM}^{(a)}[k] = \mathcal{I}\left((x_{R,f}^2(t))\right)_k^{(a)} = \overbrace{\mathcal{I}\left(u_f^2(t)\right)_k^{(a)}}^{E_k^{(a)}} + \overbrace{\mathcal{I}\left(2u_f(t)w_{R,f}(t)\right)_k^{(a)}}^{\zeta_k^{(a)}} + \overbrace{\mathcal{I}\left(w_{R,f}^2(t)\right)_k^{(a)}}^{\eta_k^{(a)}} \tag{7.12}$$

where $a \in \{0,1\}$, $E_k^{(a)}$is a useful signal energy for the k-th symbol for a time shift complying to 0 ($a=0$) or δ ($a=1$), $\zeta_k^{(a)}$ and $\eta_k^{(a)}$ are noise terms with the same properties as for BPSK.

7.1.3.2 Demodulation

We define two sets of time–windows $\mathcal{A}_k^{(0)}$ and $\mathcal{A}_k^{(1)}$ complying to the time shifts 0 and δ respectively. Then, the pulses in the transmitted signals from A and B can be present in $\mathcal{A}_k^{(0)}$ or $\mathcal{A}_k^{(1)}$ only or in $\mathcal{A}_k^{(0)}$ and in $\mathcal{A}_k^{(1)}$ simultaneously depending on the combination of $c_{A,k}$ and $c_{B,k}$.

We define events $\mathcal{E}_{0,k}^{(a)}$, $\mathcal{E}_{A,k}^{(a)}$, $\mathcal{E}_{B,k}^{(a)}$ and $\mathcal{E}_{2,k}^{(a)}$ meaning that no useful signal, useful signal from A, useful signal from B and useful signals from A and B, respectively, are present in $\mathcal{A}_k^{(a)}$ for the k-th symbol.

Then, if $c_{A,k} = c_{B,k}$ events $\mathcal{E}_{0,k}^{(a)}$ and $\mathcal{E}_{2,k}^{(a')}$ occur for $a \neq a'$. For $c_{A,k} \neq c_{B,k}$ events $\mathcal{E}_{A,k}^{(a)}$ and $\mathcal{E}_{B,k}^{(a')}$ occur for $a \neq a'$. Now we denote an event of detection of a useful signal in $\mathcal{A}_k^{(a)}$ as $\mathcal{D}_k^{(a)}$ which occurs if $i_{2PPM}^{(a)}[k] \geq T_o$ and similarly an event of non–detection $\bar{\mathcal{D}}_k^{(a)}$ which occurs when $i_{2PPM}^{(a)}[k] < T_o$. Then the strategy of detecting the codeword symbols is as follows

$$\hat{c}_{AB,k} = \begin{cases} 1; & \mathcal{D}_k^{(a)} \wedge \mathcal{D}_k^{(a')}; a \neq a' \\ 0; & \text{otherwise} \end{cases}. \tag{7.13}$$

The advantage of this demodulation strategy is an inherent robustness to the channel parametrization. This is caused by the following. If $c_{A,k} \neq c_{B,k}$ ($c_{AB,k} = 1$ according to the mapping in table 7.1), events $\mathcal{E}_{A,k}^{(a)}$ and $\mathcal{E}_{B,k}^{(a')}$ occur and since the useful signals are in different sets of frames and they do not influence each other, events $\mathcal{D}_k^{(a)}$ and $\mathcal{D}_k^{(a')}$ occur with high probability. if $c_{A,k} = c_{B,k}$, useful signals are both in the same set of frames $\mathcal{A}_k^{(a)}$ and thus influence $i_{2PPM}^{(a)}[k]$ through the mutual energy as in the case of BPSK. However, this influence does not affect negatively the estimate of $c_{AB,k}$ — $\hat{c}_{AB,k}$. This is caused by the fact that if $c_{A,k} = c_{B,k}$, an error occurs if $\mathcal{D}_k^{(a)}$ and $\mathcal{D}_k^{(a')}$ both occur. But one set of frames contains only noise and so a detection of signal in that set of frames is of a low probability (depending on SNR).

7.1.4 Numerical Results

We assume that the transmitted pulse is

$$p_t(t) = C\left(\frac{16\pi^2 t^2}{\tau^4} - \frac{4\pi}{\tau^2}\right) e^{-2\pi\left(\frac{t}{\tau}\right)^2} \tag{7.14}$$

which is a 2nd derivative of a Gaussian pulse. In (7.14), C is an energy normalization constant, τ is a time parameter which was assumed $\tau = 2$ ns. Channels from A and B were modeled by IEEE 802.15.3a CM1 multipath channel models (see [10]). We assumed $N_f = 1$. Cut–off frequencies of the input bandpass filter were set so as to filter out the frequencies with the PSD decrease greater or equal to 40 dB to the maximum in the transmitted signal. We assumed that individual frames of the useful signal are energetically independent of the other frames which leads to an assumption of zero inter–symbol interference (ISI). We also assumed an integration interval $T_I = 2\tau_{RMS}$ where τ_{RMS} is a RMS delay spread of the channel.

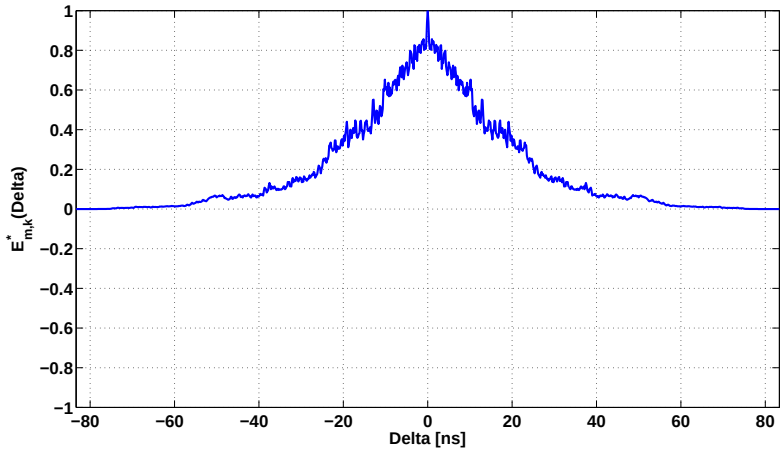

Figure 7.2: Dependence of $E^*_{m,k}(\Delta)$ on Δ

7.1.4.1 Mutual Energy Investigation

Since the mutual energy is important because it affects the decision variables and in case of BPSK the principle of demodulation relies on a high absolute value of the mutual energy, we investigate its value for a time–shift of the signals from A and B Δ caused by the imperfect time–synchronization of the nodes. We define

$$E^*_{m,k}(\Delta) = \max_{i,j} \left| \mathcal{I} \left(\left(p_t(t) * h_A^{(i)}(t) \right) \left(p(t-\Delta) * h_B^{(j)}(t) \right) \right)_k \right| \tag{7.15}$$

where i and j denote indices of channel impulse responses picked up from 100 realizations of IEEE 802.15.3a CM1 model, forming 10^4 possible combinations. Thus, $E^*_{m,k}(\Delta)$ is a maximal absolute value of the mutual energy of the useful signals at R for a given time–shift. We can see that the greater the Δ is, the lower $E^*_{m,k}(\Delta)$ is. Though roughly, we can infer that for great values of Δ, BPSK will not have a good performance.

7.1.4.2 BPSK

We first investigate the effect of mutual energy on the performance of BPSK. Dependence of performance on $E_{m,k}$ is depicted in figure 7.3 where E_b is an energy of the useful signal from user A per bit and N_0 is a power spectral density.

We can see that the lower $E_{m,k}$ is, the worse performance BPSK relay receiver has, indeed.

Moreover, simulations over 10^4 combinations of channel impulse responses $h_A(t)$ and $h_B(t)$ were performed which show the average capacity for two different time–shifts.. Results of simulations are depicted in the figure 7.4.

As we can see from the figure 7.4, non–zero time–shift has a disastrous effect on the performance of BPSK. This consequences into a necessity of very good time–synchronization of the nodes in 2WRC.

7.1.4.3 2PPM

Figure 7.5 depicts a dependence of performance of 2PPM for different values of the mutual energy. We can see from the figure that dependence is practically negligible.

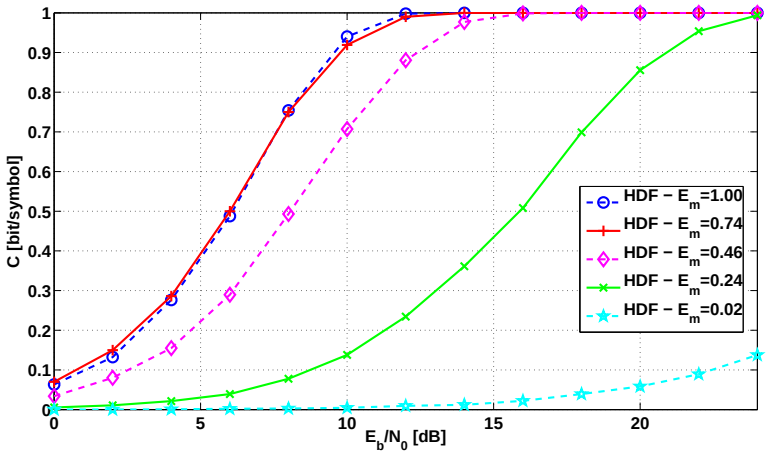

Figure 7.3: Dependence of performance of BPSK on $E_{m,k}$

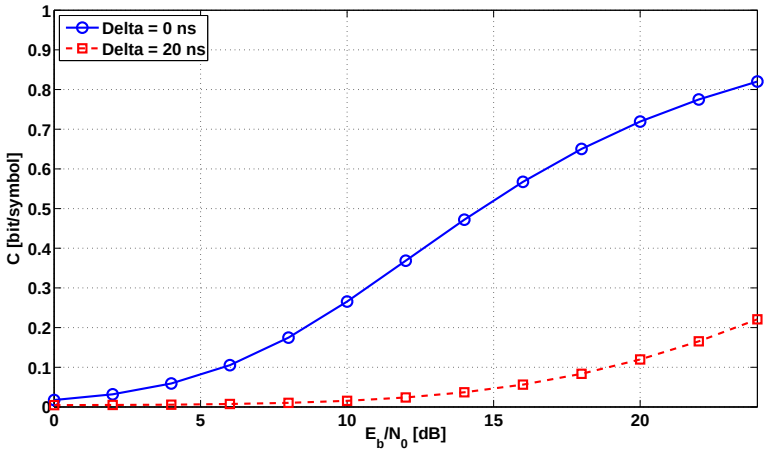

Figure 7.4: Averaged capacity of BPSK for two time–shifts

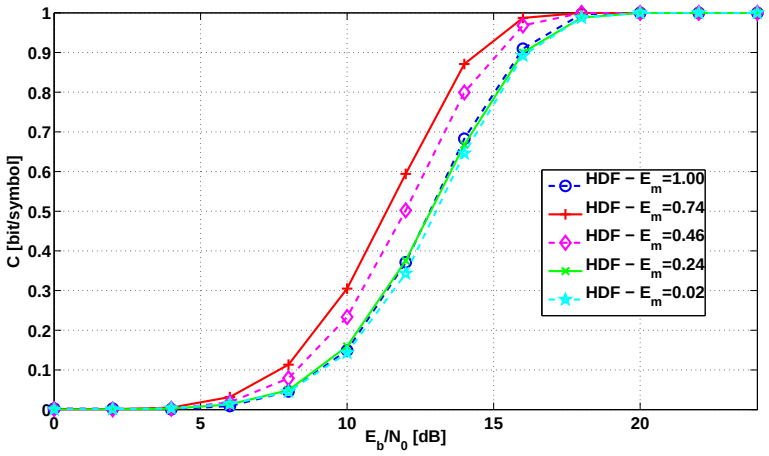

Figure 7.5: Dependence of performance of 2PPM on $E_{m,k}$

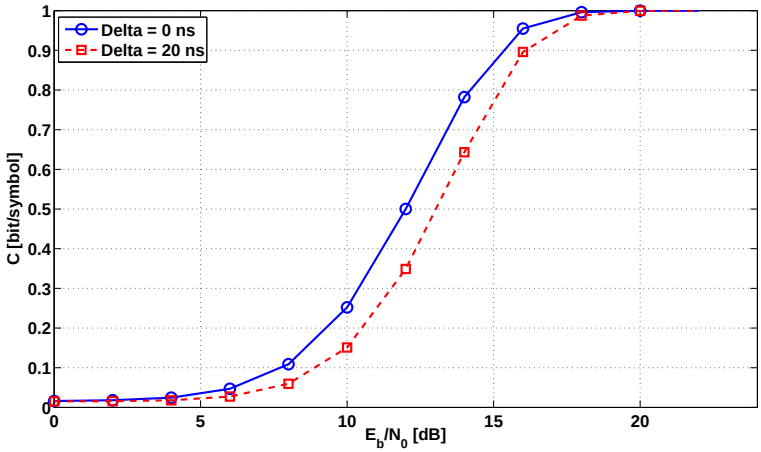

Figure 7.6: Averaged capacity of 2PPM for two time–shifts

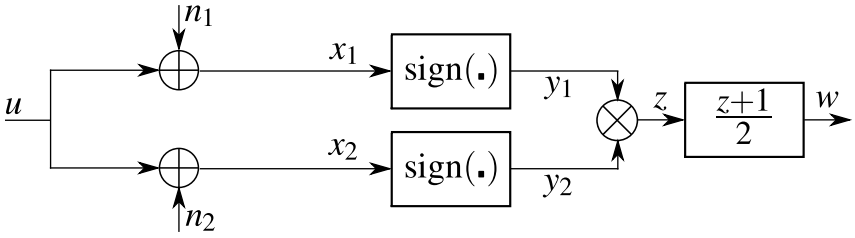

Figure 7.7: LDR platform

Figure 7.6 provides a comparison of performance of 2PPM for two different time–shifts Δ. We can see that the results slightly differ which is caused by the fact that the integration interval is longer for $\Delta = 20$ ns which causes a greater noise variance.

7.2 LDR Receiver

7.2.1 Receiver Structure

In this section we will assume a Low Data Rate (LDR) receiver platform [9]. This is in fact a non-coherent energy detector for the UWB signals. We will use a term energy although due to its specific signal processing the receiver do not evaluate the energy in the strict sense. Its formal signal processing flow is depicted on Fig. 7.7. The useful received signal – for BPSK and 2PPM given by (4.3) and (4.5), respectively – is divided into two similar branches in the receiver. In each the AWGN is added. Due to the different path through the receiver noises n_1, n_2 are assumed to be uncorrelated. Noisy signals x_1, x_2 are then amplified to the limitation which is equivalent to the sign$(\cdot)$ operation. This can be also seen as a 1bit analog to digital conversion. Bipolar signals $y_1, y_2 \in \{-1, 1\}$ are multiplied together – by this we obtain the "energy" of the signal $z \in \{-1, 1\}$. The bipolar signal z is simply transformed to the binary signal $w \in \{0, 1\}$. The receiver output w is sampled with sampling frequency about 1 GHz. Note that this frequency is significantly below the Nyquist condition, but signal samples are not used for the reconstruction of the signal they only carry the information about the "energy" of the signal.

The discrete receiver output $w[k]$ is summed up over a priory given time interval – an in-

q_{AB}	$q_A = 0$	$q_A = 1$
$q_B = 0$	1	0
$q_B = 1$	0	1

Table 7.2: Minimal Hierarchical eXclusive mapping for LDR

tegration interval T_I – which consist of N_P consecutive signal samples. Decision about the hierarchical symbols are performed on this summation $S = \sum_{k=0}^{N_P-1} w[k]$.

7.2.2 Capacity Evaluation

The evaluation of the MAC capacity proceeds in the very similar way as described in Section 4.3.2 taking the specific signal processing of the LDR platform into account. We evaluate the MAC capacity for BPSK as well as 2PPM modulation.

7.2.2.1 BPSK Modulation

We assume the minimal hierarchical exclusive mapping given by Tab. 7.2 where q_A, q_B are transmitted symbols and q_{AB} is the hierarchical symbol.

For evaluation of the system performance we have to evaluate probability mass functions of the k-th sample of the output signal w. We evaluate this probabilities conditioned by the hierarchical symbol q_{AB} i.e.

$$p(w[k] = 0|q_{AB} = 0) \tag{7.16}$$

$$p(w[k] = 0|q_{AB} = 1) \tag{7.17}$$

The probability7.16 is given by

$$\begin{aligned} p(w[k] = 0|q_{AB} = 0) \quad = \quad & p(y_1[k] = 1|q_{AB} = 0)p(y_2[k] = -1|q_{AB} = 0) + \\ & + p(y_1[k] = -1|q_{AB} = 0)p(y_2[k] = 1|q_{AB} = 0) \end{aligned} \tag{7.18}$$

Noises n_1, n_2 are AWGN $\sim \mathcal{N}(0, \sigma^2)$. Under this assumption we have

$$p(y_i[k] = 1|q_{AB} = 0) = p(u_{|q_{AB}=0}[k] \geq n_i[k]) = Q\left(\frac{-u_{|q_{AB}=0}[k]}{\sigma}\right) \tag{7.19}$$

$$p(y_i[k] = -1|q_{AB} = 0) = p(u_{|q_{AB}=0}[k] < n_i[k]) = 1 - Q\left(\frac{-u_{|q_{AB}=0}[k]}{\sigma}\right) \tag{7.20}$$

where $i \in \{1, 2\}$ and $Q(x) = \frac{1}{\sqrt{2\pi}} \int_x^\infty \exp\left(-\frac{v^2}{2}\right) \mathrm{d}v$. Informally we evaluate the probability whether the sample of noise $n[k]$ changes the polarity (the sign) of the useful signal sample $u_{|q_{AB}=0}[k]$.

Substituting this into 7.18 we obtain

$$p(w[k] = 0|q_{AB} = 0) = 2Q\left(\frac{-u_{|q_{AB}=0}[k]}{\sigma}\right)\left(1 - Q\left(\frac{-u_{|q_{AB}=0}[k]}{\sigma}\right)\right) \tag{7.21}$$

The evaluation of the probability in 7.17proceeds in the similar way

$$p(w[k] = 0|q_{AB} = 1) = 2Q\left(\frac{-u_{|q_{AB}=1}[k]}{\sigma}\right)\left(1 - Q\left(\frac{-u_{|q_{AB}=1}[k]}{\sigma}\right)\right) \tag{7.22}$$

The receiver sums the N_P samples of the output $w[k]$ which belong to the given integration interval T_I to obtain the decision variable $S = \sum_{k=0}^{N_P-1} w[k]$. In order to set the appropriate

threshold level T we investigate the conditioned probabilities $p(S|q_{AB}=0)$ and $p(S|q_{AB}=1)$. Individual samples are mutually independent thus $p(S|q_{AB}=0) = p(w[0]|q_{AB}=0) * \cdots * p(w[N_P-1]|q_{AB}=0)$, where $*$ is the convolution. Similarly for the probability $p(S|q_{AB}=1)$.

This forms the asymmetric binary channel depicted on Fig. 4.2. With transition probabilities $p_{10} = p(S \leq T|q_{AB}=1) = \sum_{i=0}^{T-1} p(S=i|q_{AB}=1)$ and $p_{01} = p(S > T|q_{AB}=0) = \sum_{i=T}^{N_P-1} p(S=i|q_{AB}=0)$.

Threshold level T and hence the transition probabilities are optimized for every SNR to maximize the channel capacity according to the principles described in Section 4.3.2.

The channel capacity for given threshold level and given transition probabilities p_{01}, p_{10} is $C = H(\hat{q}_{AB}) - H(\hat{q}_{AB}|q_{AB})$. Where entropies $H(\cdot)$ are

$$\begin{aligned} H(\hat{q}_{AB}) &= -\frac{1}{2}(1-p_{01}+p_{10})\log_2\frac{1}{2}(1-p_{01}+p_{10}) - \\ &\quad -\frac{1}{2}(1-p_{10}+p_{01})\log_2\frac{1}{2}(1-p_{10}+p_{01}) \end{aligned}$$

$$\begin{aligned} H(\hat{q}_{AB}|q_{AB}) &= -\frac{1}{2}(1-p_{01})\log_2(1-p_{01}) - \frac{1}{2}p_{01}\log_2 p_{01} - \\ &\quad -\frac{1}{2}(1-p_{10})\log_2(1-p_{10}) - \frac{1}{2}p_{10}\log_2 p_{10} \end{aligned}$$

7.2.2.2 N-ary PPM Modulation

The MAC capacity for PPM modulation proceeds in the following way. For every PPM time slot three situation can happen: zero, one or two pulses can be transmitted within it. Based on appropriately chosen threshold level T – derived similarly to BPSK case – the receiver makes the hard decision about the presence or not presence of the transmission for every PPM time slot.

Final decision about the whole symbol is obtained by simple combinatorial rules from hard decisions. Concretely, if there is only one time slot with detected energy in it the relay makes decision that both users transmit the same symbol corresponding to the time slot and so on. This forms the binary asymmetric channel with appropriate transition probabilities from which we evaluate the MAC capacity.

7.2.3 Numerical Results

By the numerical simulation the MAC capacity for BPSK and 2PPM modulation was evaluated. To model the CIR we adopt various kinds of the Modified Saleh-Valenzuela channel model. This channel model is recommended by IEEE 802.15 as a channel for WPANs including UWB technology [10].

We investigate the impact of various channel realizations of channel $A \to R, B \to R$ on the MAC stage capacity. As a measure of similarity the mutual energy $E_m = \langle p_A(t); p_B(t)\rangle$was used, where $\langle\cdot\rangle$is properly defined inner scalar product and $p_A(t), p_B(t)$ are waveforms at the input of the relay R. Received signal were normalized to obtain $||p_A(t)||^2 = ||p_B(t)||^2 = 1$.

Second derivative of Gaussian pulse according (7.14) was used as a transmitted pulse.

7.2.3.1 BPSK

Figures 7.8, 7.9 and 7.10 show the MAC capacity as a function of SNR for BPSK modulation for various kinds of channel models. Capacity is evaluated for several channel pairs, appropriate mutual energy E_m is noted in the legend.

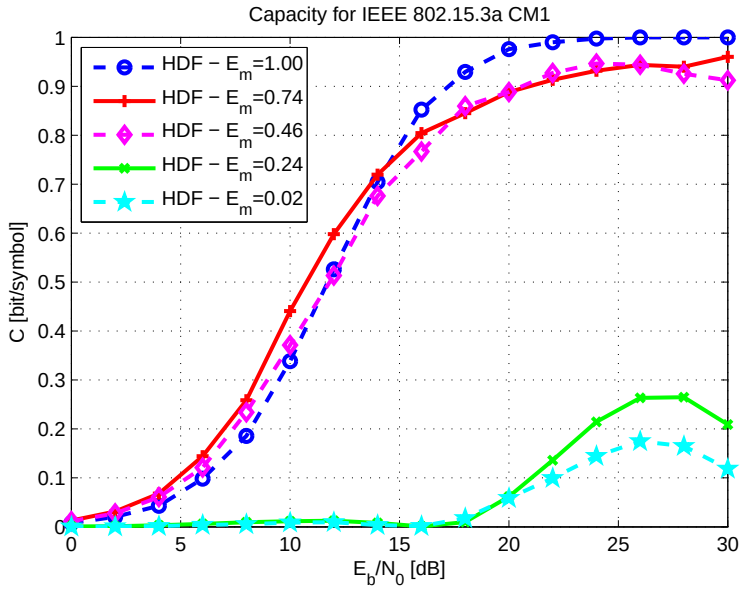

Figure 7.8: MAC capacity for BPSK - CM1

We can see the significant impact of E_m on the MAC capacity. Generally when $E_m \to 0$ the performance is catastrophic. This behavior is observed for all channel models. As a direct consequence the BPSK modulation needs the perfect time synchronization of the transmissions, otherwise any asynchronism will cause $E_m \to 0$ and thus degradation of the channel capacity. The impact of the synchronization on the mutual energy is depicted on Fig. 7.2.

7.2.3.2 2PPM

Figures 7.11, 7.12 and 7.13 show the MAC capacity as a function of SNR for 2PPM modulation for various kinds of channel models. Capacity is evaluated for several channel pairs, appropriate mutual energy E_m is noted in the legend.

The impact of different channel realization is not so significant as in the BPSK case. Especially when $E_m \to 0$ the system performance is still good. As a consequence the 2PPM modulation is expected to by invariant to the imperfect synchronization of the sources. On the other hand if we compare the results for the same channel model we can see that for similar channels, i.e. $E_m \to 1$, BPSK outperforms 2PPM modulation.

Generally the necessity of high SNR to achieve the full capacity of the used modulation (1 bit/symbol in the case of BPSK and 2PPM) is a price that is payed for the suboptimal energy detector receiver structure.

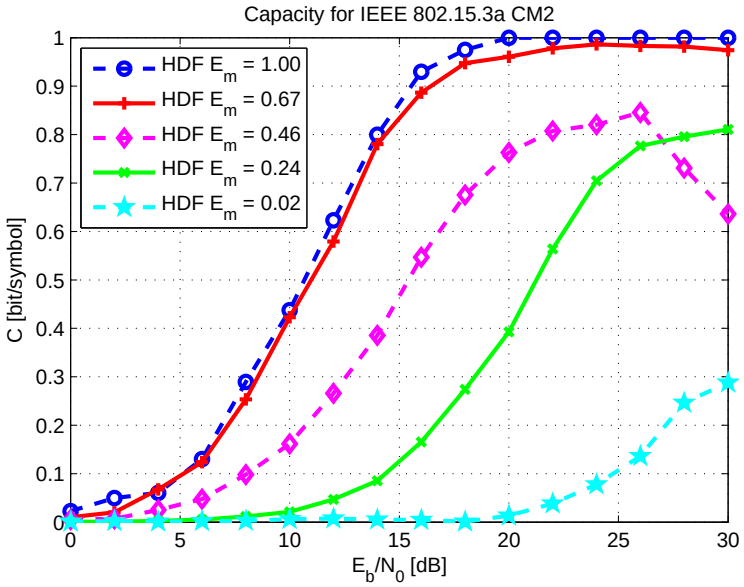

Figure 7.9: MAC capacity for BPSK - CM2

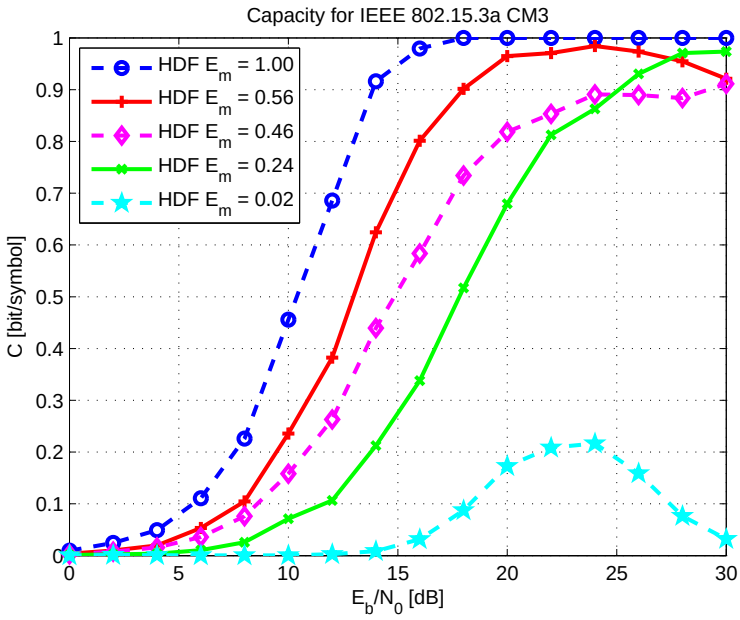

Figure 7.10: MAC capacity for BPSK - CM3

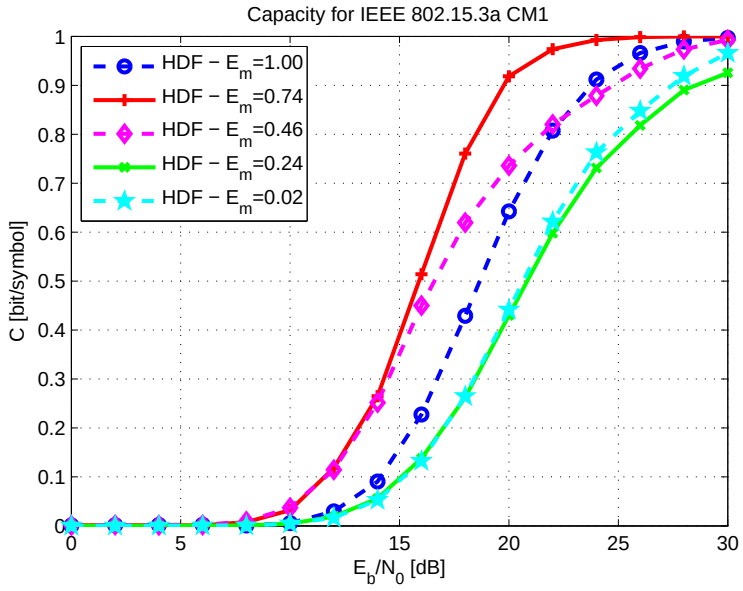

Figure 7.11: MAC capacity for 2PPM - CM1

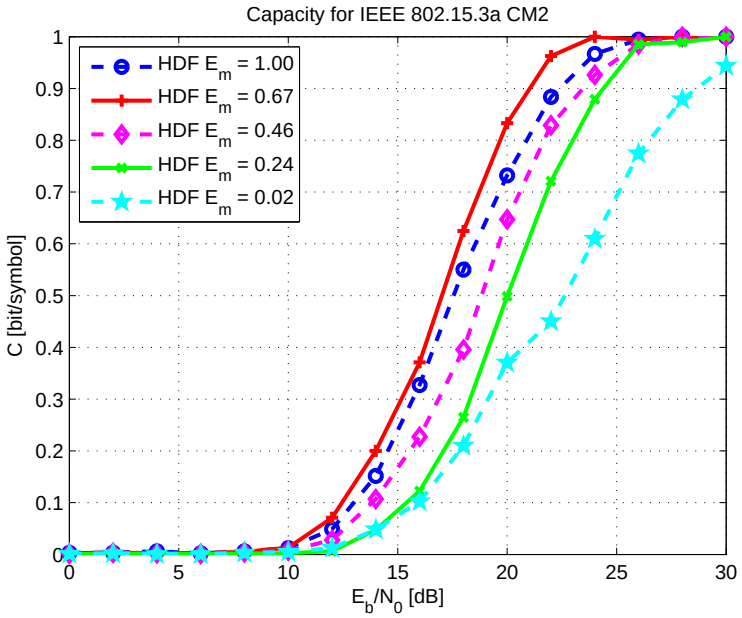

Figure 7.12: MAC capacity for 2PPM - CM2

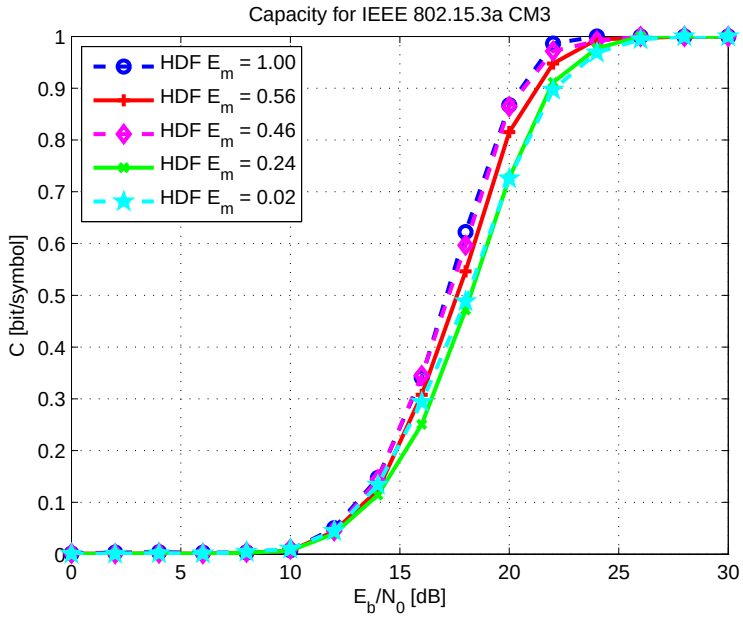

Figure 7.13: MAC capacity for 2PPM - CM3

8 Comparison of HDF and Non–HDF Approach

8.1 Coherent Receiver

In this chapter we summarize the gain of the application of the HDF strategy over the JDF strategy and over the orthogonal concept for the coherent receiver described in Chapter 6. The gain is illustrated on the MAC capacity regions.

8.1.1 HDF vs. JDF

Fig. 8.1 shows the capacity regions of the HDF (in red) and the JDF (in green) strategy for 2PPM modulation for a composite signal subspace. The capacity regions are obtained as cuts for a given SNR of the MAC capacity depicted in 6.9. The capacity region C_{AB} of HDF strategy has a rectangular shape [16]. In our case, due to the assumed symmetry of the source relay links, has a square shape. JDF capacity region is given by the first and the second order cut-set bounds. The first order cut-set bound – C_0 – is in fact a pure single user capacity whilst the second order cut-set bound – C_S – is a sum rate rescaled to one user. Note that we assume the same rates of both users as well as the symmetric channels $SA \rightarrow R$ and $SB \rightarrow R$. The shape of the JDF capacity region is generally rectangular with trimmed uppermost corner.

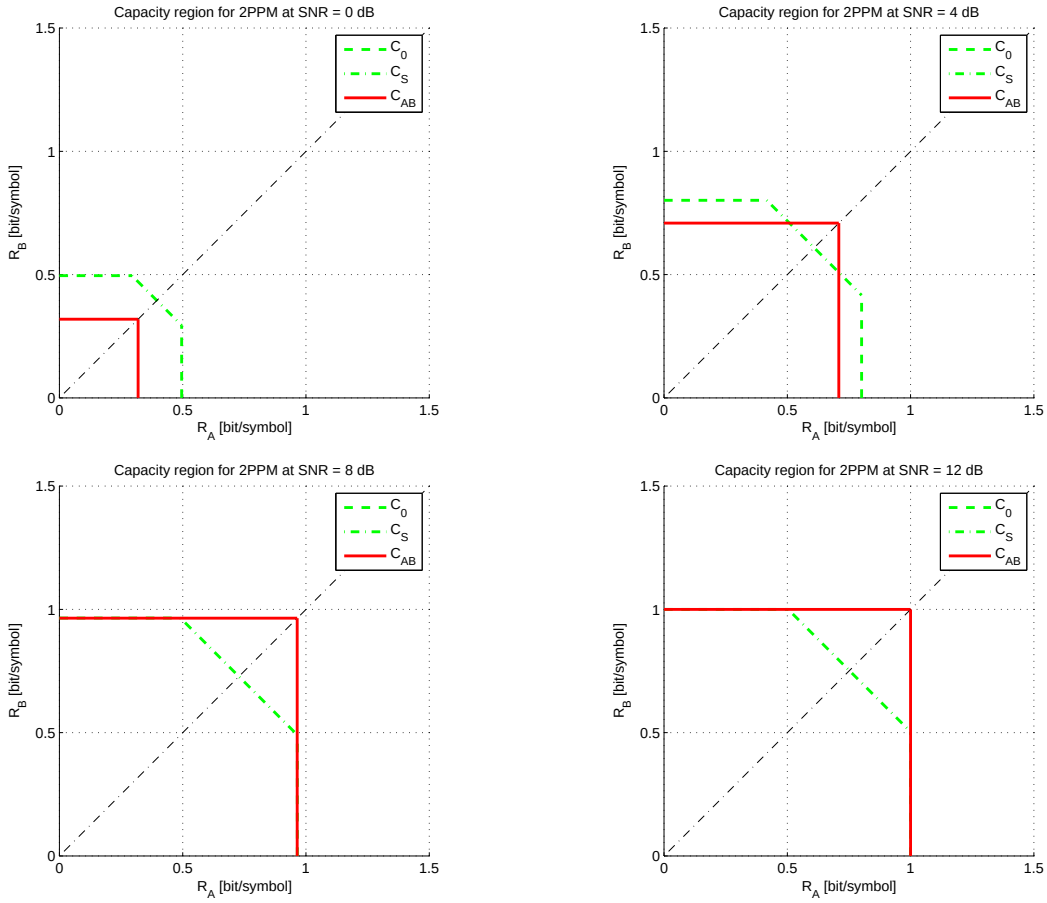

Figure 8.1: HDF and JDF capacity regions

From a comparison depicted in Fig. 8.1 the advantage of the HDF over the JDF strategy can be seen. The HDF capacity region for a sufficiently large SNR exceeds beyond the JDF capacity region. Thus HDF offers a higher sum rate. For a low SNR there is a gap between the single user capacity C_0 and the HDF capacity – the gap between the red and the green dashed line of Fig. 8.1. With growing SNR this gap diminished until for sufficient a SNR these two capacities coincide. In the SNR region where the capacity is limited by the source alphabet cardinality the HDF strategy offers a full capacity (we assume the same cardinality of both sources) while the capacity offered by the JDF to one user is significantly lower.

8.1.2 HDF vs. Orthogonal Separation

In this part we will compare the HDF strategy with perfectly orthogonally separated users. Due to the UWB technology we will assume a TDM and CDM user separation. Separation in frequency will need different transmitted pulse shape for every source and this was not expected during the evaluation of the capacity. Due to the same reasons we do not mention any other pulse shape modulation.

The first comparison will be between the HDF strategy and two users separated by CDM transmitted within the same time instants. Because the perfect orthogonality between the transition the capacity of each user is given by the SNR of its link to the relay node. The capacity region of such a communication will be rectangular. We can obtain it simply from the Fig. 8.1 by ignoring the second order cut-set bound C_S – green dash-and-dot line and by

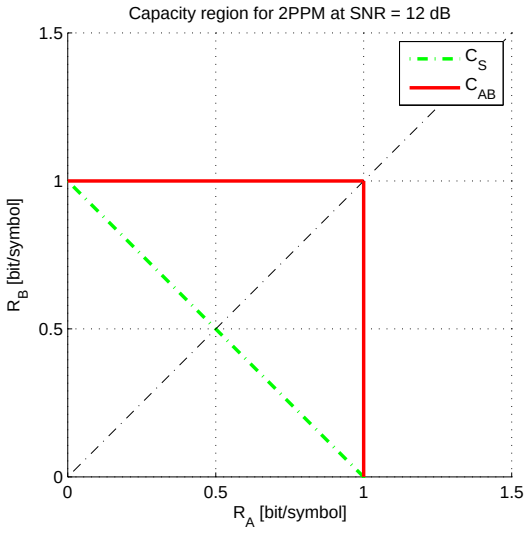

Figure 8.2: HDF and time sharing capacity regions

extension of first order cut-set bound C_0 to form a rectangle. For a low SNR this capacity region is beyond the HDF one. For a large SNR the capacity regions coincide and are limited by the source cardinality. But we still have to keep in mind that the rectangular shape for separated users is possible only due to the perfect orthogonal separation. We spend double amount of available resources (two orthogonal codes in this case) than in the HDF case.

The second comparison will be between the HDF strategy and two user separated in time. Similarly to the CDM case a TDM capacity region for sufficient large SNR will be the same as the HDF one. But we need twice more time to achieve it. If we have got only the one time instant with the same length as for HDF strategy, the only way is proportional time sharing [2]. The resulting capacity region will be triangular and will offer substantially lower capacity than the HDF strategy. The example of the capacity region with the time sharing is depicted on Fig. 8.2.

8.2 Non–Coherent Receiver

Concerning a non–coherent receiver, the possibilities of comparison HDF and other approaches to multi–user communication are much more limited than for a coherent receiver. Results and descriptions included in this section assume integration receiver.

8.2.1 HDF vs. JDF

In case of HDF vs. JDF, the possibilities of comparison are zero. JDF requires that the receiver is able to distinguish both data from A and B. However, this is a problem because a non–coherent HDF IR–UWB receiver is based on a simple pulse detection. In case of BPSK using an energy detector, the decision variable for k-th symbol is of a form, see (7.3),

$$\begin{aligned} i_{BPKS}[k] &= \mathcal{I}\left(u_f^2(t)\right)_k + 2\mathcal{I}\left(u_f(t)w_{R,f}(t)\right)_k + \mathcal{I}\left(w_{R,f}^2(t)\right)_k \\ &= E_{A,k} + E_{B,k} + 2q'_{A,k}q'_{B,k}E_{m,k} + \zeta_k + \eta_k \end{aligned} \tag{8.1}$$

where $\zeta_k$and η_k are noise terms, $E_{A,k}$, $E_{B,k}$ are symbol energies for A and B, respectively, and $E_{m,k}$is a mutual energy of signals from A and B. As we can see, the receiver cannot distinguish

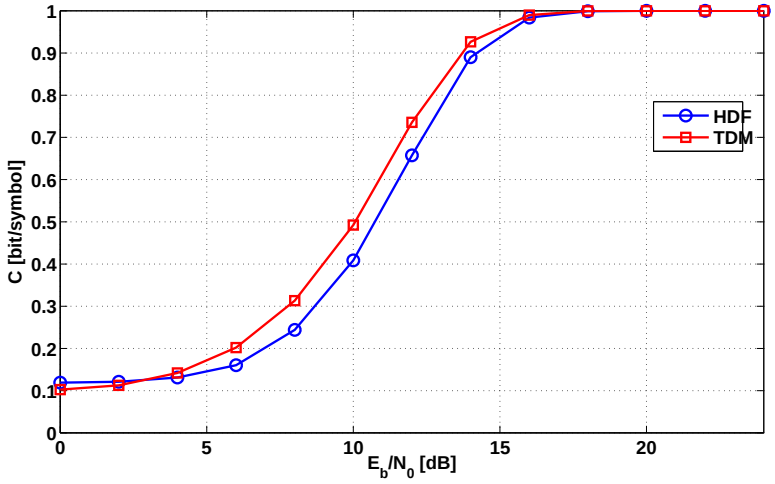

Figure 8.3: Comparison of HDF and TDM for 2PPM

e.g. cases $\{d_{A,k}=0, d_{B,k}=1\}$, resulting in $\left(q'_{A,k}=-1, q'_{B,k}=1\right)$, and $\{d_{A,k}=1, d_{B,k}=0\}$, resulting in $\left(q'_{A,k}=1, q'_{B,k}=-1\right)$. This results into a impossibility to use JDF and compare with HDF.

Let us pay our attention to a case of 2PPM. If only one pulse is detected, the receiver believes that both pulses are present in a given frame. But if a presence of a useful signal is detected in both frames, the receiver cannot distinguish the source of the signals since it only detects the *presence* of a useful signal.

8.2.2 HDF vs. Orthogonal Separation

As well as for HDF vs. JDF case, in HDF vs. orthogonal separation case, fair comparison possibilities are not broad for a non–coherent receiver.

Considering CDM separation, BPSK cannot be used this way because if signals $u_A(t)$ and $u_B(t)$ are orthogonal in sense $\mathcal{I}\left(u_A(t)u_B(t)\right)_k = 0$ then

$$\begin{aligned} i_{BPSK}[k] &= \mathcal{I}\left(u_f^2(t)\right)_k + 2\mathcal{I}\left(u_f(t)w_{R,f}(t)\right)_k + \mathcal{I}\left(w_{R,f}^2(t)\right)_k \\ &= \mathcal{I}\left(u_{A,f}^2(t)\right)_k + \mathcal{I}\left(u_{B,f}^2(t)\right)_k + \overbrace{\mathcal{I}\left(u_{A,f}(t)u_{B,f}(t)\right)_k}^{0} + \zeta_k + \eta_k \\ &= E_{A,k} + E_{B,k} + \zeta_k + \eta_k \end{aligned} \tag{8.2}$$

which results into the fact that the receiver cannot distinguish e.g. cases $\{d_{A,k}=0, d_{B,k}=1\}$, resulting in $\left(q'_{A,k}=-1, q'_{B,k}=1\right)$, and $\{d_{A,k}=1, d_{B,k}=0\}$, resulting in $\left(q'_{A,k}=1, q'_{B,k}=-1\right)$ because $i_{BPSK}[k]$ does not depend on data. A case of 2PPM is not dealt with here.

If we consider TDM, it is not possible to use BPSK because this would mean a demodulation of two separate signals. This is the problem because BPSK cannot be demodulated with a non–coherent receiver.

2PPM can be compared in terms of HDF vs. TDM. The capacity is depicted in figure 8.3. It is evident that TDM needs slightly lower SNR but we must keep in mind that the symbol length for TDM is twice longer than for HDF which affects data rates per second.

9 Conclusion

This report summarizes the results of the Task 2.4.2 of the EUWB project. This task investigates the physical layer of the UWB communication system utilizing the knowledge of the network structure. Instead of interference mitigation/avoidance techniques this approach takes mutual interferences into account in the design procedure of the modulation, coding and signal processing. Task 2.4.2. investigates techniques and methods for channel and resource sharing based on the Wireless Network Coding mechanisms with Hierarchical Decode and Forward strategy. The main contributions are:

- adaptation of WNC with the HDF strategy on the UWB specific technology,
- mathematical derivation of MAC stage capacity of 2WRC,
- assuming various kind of the receiver signal processing including:
  - coherent approach – represented by the receiver with subspace projection,
  - non-coherent approach – based on various forms of energy detectors,
- numerical evaluation of the MAC stage capacity for UWB channel parameterization.

Result presented in this report were published in:

- Tomas Hynek and Jan Sykora. Hierarchical decode & forward strategy in IR-UWB communication systems. In *Proc. Future Network and MobileSummit 2011*, Warsaw, Poland, June 2011.
- Tomas Hynek and Jan Sykora. Capacity regions of wireless network coding with hierarchical decode & forward strategy applied on impulse radio UWB technology. In *Proc. IEEE International Conference on Ultra-Wideband (ICUWB)*, Bologna, Italy, September 2011.
- Martin Masek and Jan Sykora. Hierarchical decode and forward strategy in energy-detector based non-coherent impulse-radio ultra-wideband systems. *IET Communications* . Submitted for publication.

Bibliography

[1] Commission of the European Communities. Commission decision of 21 February 2007 on allowing the use of the radio spectrum for equipment using ultra-wideband technology in a harmonised manner in the community (2007/131/EC). Online: `http://eur-lex.europa.eu/`. Official Journal of the European Union, Feb. 23, 2007.

[2] Thomas M. Cover and Joy A. Thomas. *Elements of Information Theory*. John Willey & Sons, Inc., 1991.

[3] Andrea Giorgetti et al. EUWB deliverable 2.2.1. Online: `http://www.euwb.eu`, 2009.

[4] Andrea Giorgetti et al. EUWB deliverable 2.3.1. Online: `http://www.euwb.eu`, 2010.

[5] Andrea Giorgetti et al. EUWB deliverable 2.4.2. Online: `http://www.euwb.eu`, 2010.

[6] Andrea Giorgetti et al. EUWB deliverable 2.4.4. Online: `http://www.euwb.eu`, 2011.

[7] Andrea Mariani et al. EUWB deliverable 2.2.2. Online: `http://www.euwb.eu`, 2010.

[8] Andrea Mariani et al. EUWB deliverable 2.2.3. Online: `http://www.euwb.eu`, 2010.

[9] Manuel Pezzin et al. EUWB deliverable 7.1.1b v1.0. Online: `http://www.euwb.eu`, 2010.

[10] Jeff Foerster. Channel modeling sub-committee report final. Technical report, IEEE P802.15 Working Group for Wireless Personal Area Networks (WPANs), November 2002.

[11] M. Ghavami, L. B. Michael, and R. Kohno. *Ultra Wideband Signals and Systems in Communication Engineering*. John Wiley & sons, Ltd., 2nd edition, 2007.

[12] Tomas Hynek and Jan Sykora. Capacity regions of wireless network coding with hierarchical decode & forward strategy applied on impulse radio UWB technology. In *Proc. IEEE International Conference on Ultra-Wideband (ICUWB)*, Bologna, Italy, September 2011.

[13] Martin Masek and Jan Sykora. Hierarchical decode and forward strategy in energy-detector-based non-coherent impulse-radio ultra-wideband systems. *IET Communications*. Submitted for publication.

[14] Jan Sykora and Alister Burr. Hierarchical alphabet and parametric channel constrained capacity regions for hdf strategy in parametric wireless 2-wrc. In *Proc. IEEE Wireless Commun. Network. Conf. (WCNC)*, pages 1–6, April 2010.

[15] Jan Sykora and Alister Burr. Network coded modulation with partial side-information and hierarchical decode and forward relay sharing in multi-source wireless network. In *Proc. European Wireless Conf. (EW)*, pages 1–7, April 2010.

[16] Jan Sykora and Alister Burr. Layered design of hierarchical exclusive codebook and its capacity regions for HDF strategy in parametric wireless 2-WRC. *Vehicular Technology, IEEE Transactions on*, PP(99), 2011.

[17] Tomas Uricar and Jan Sykora. Design criteria for hierarchical exclusive code with parameter-invariant decision regions for wireless 2-way relay channel. *EURASIP J. Wireless Comm. and Networking*, 2010.

[18] Klaus Witrisal, Geert Leus, Gerard J. M. Janssen, Marco Pausini, Florian Troesch, Thomas Zasowski, and Jac Romme. Noncoherent ultra-wideband systems. *IEEE Signal Processing Magazine*, pages 48–66, July 2009.

[19] Liuqing Yang and Georgios B. Giannakis. Ultra-wideband communications. *IEEE Signal Processing Magazine*, pages 26–54, November 2004.